Developing a Small Molecule Regulated Cre Recombinase
and
A Chemical-Genetic Strategy for the Investigation of Kinase Non-Catalytic Function using Covalent Conformation-Selective Inhibitors

Bridget Marley Trevillian
A dissertation
submitted in partial fulfillment of the
requirements for the degree of

Doctor of Philosophy

University of Washington

2016

Reading Committee:

Dustin J. Maly, Chair

Michael Gelb

Champak Chatterjee

Program authorized to offer degree:

Chemistry
University of Washington

Abstract:

Developing a Small Molecule Regulated Cre Recombinase
and
A Chemical-Genetic Strategy for the Investigation of Kinase Non-Catalytic Function using Covalent Conformation-Selective Inhibitors

Bridget Marley Trevillain

Chair of Supervisory Committee:
Professor Dustin J. Maly
Department of Chemistry

Chapter 1: Developing a Small Molecule Regulated Cre Recombinase

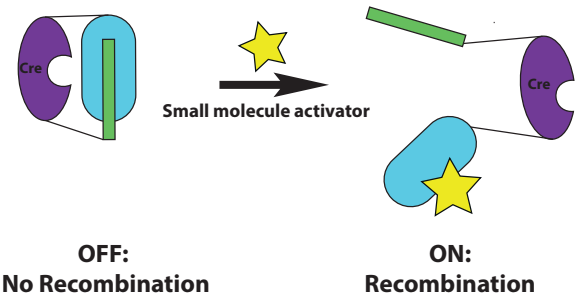

Figure I-1: Synthetically Regulated Cre Recombinase

A chemical genetic method for controlling signaling enzymes has previously been developed in our lab. In this method, naturally occurring regulatory domains are replaced by a protein-protein interaction that acts as synthetic regulatory domains. This synthetically controlled signaling enzyme can be controlled by a potent, selective and cell permeable small molecule activator that disrupts the interaction of the artificial regulatory domains. Cre Recombinse (Causes Recombination) is a site-specific tyrosine recombinase from bacteriophage P1. Cre is commonly used to facilitate conditional knock-in, knock-out and inversion

studies is mammals[8]. Our goal is to control the function of Cre Recombinase in cells and in animals using our synthetically activated switch. The synthetically controlled Cre recombinase will be used to conditionally activate or inactivate gene expression A in vivo in a tissue-specific manner with both spatial and temporal control. Towards this goal, we have developed a well controlled synthetically regulated Cre recombinase that is tightly auto-inhibited, but has a high activation in mammalian cells. In this work, we determine the mechanism of autoinhibition and also take the first steps towards using this system in mice.

Chapter 2: A Chemical-Genetic Strategy for the Investigation of Kinase Non-Catalytic Function using Covalent Conformation-Selective Inhibitors

Protein kinases are a large family of 518 signaling proteins that allow a cell to respond appropriately to a variety of external stimuli (Manning et. al. 2002). Most current research on protein kinases focuses on catalytic activity, but recent evidence has shown that the non-catalytic role of kinases is essential to cell survival, including scaffolding and DNA binding (Rauch et. al 2011). A major challenge of working with protein kinases is the lack of selective small molecule inhibitors caused by high structural homology. As a result, these non-catalytic functions have not been thoroughly investigated.

A major focus of research in the field has been development of inhibitors that selectively bind distinct ATP-binding site conformations of kinases. Specifically, Type I inhibitors (Taylor et al, 2011), which bind the catalytically active kinase, and type II inhibitors which bind to the catalytically inactive forms of the

kinase (Ranjitkar et al, 2010; Ranjitkar et al, 2014; Seeliger et al, 2009; Okram et al, 2006). In kinases, the active site conformation and regulatory domains are allosterically coupled. Stabilizing the active site of the kinase using conformationally specific inhibitors not only causes divergent signaling effects, but also impact the non-catalytic roles of protein kinases in the cell (Rauch et al, 2011). The second half of this thesis describes work analyzing the divergent impacts of conformationally selective inhibitors on non-catalytic functions of Src Family Kinases (SFKs) in cells.

Table of Contents

LIST OF FIGURES

CHAPTER 1

CHAPTER 2

Chapter 1: Developing a Small Molecule Regulated Cre Recombinase

I. Introduction

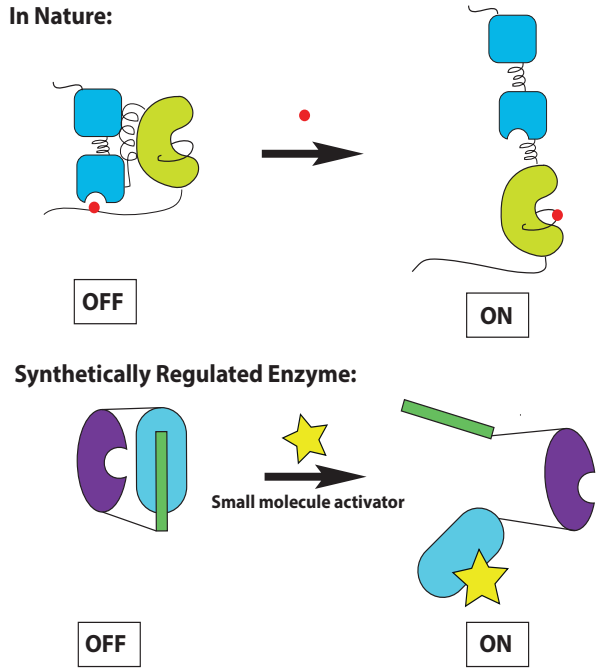

Figure 1-1: General design of small molecule regulated Cre A. Regulation of signaling enzymes in nature. **B.** Regulation of synthetic signaling enzyme using a protein protein interaction that can be disrupted by a small molecule as the non-natural regulatory domains.

One of the major goals in chemical biology is to develop small molecules that inhibit protein function. These inhibitors give rapid, reversible and dose-dependent control of protein function. Small molecules are readily absorbed into cells and can be used to inhibit protein function in minutes. It is also possible to get a graded response of protein function by using a titration of a small molecule inhibitor. Unfortunately, there is no general way to develop small molecule

inhibitors[1]. For this reason, it would be useful to have a general chemical genetic method of control of gain of function and loss of function studies.

Our lab set out to design a system in which signaling enzymes could be controlled by a small molecule in a general way[2]. In order to design such a method, the way in which nature regulates some types of signaling enzymes was observed. In nature, signaling enzymes have regulatory domains that inhibit the function of the catalytic domain, many times causing a conformational change in the active site of the enzyme. A chemical modification, such as phosphorylation event, disrupts the interaction of the regulatory domains and releases the catalytic domain, which is then free to perform it's function. Keeping in mind how nature has designed signaling enzymes, a method was developed in which a synthetic signaling enzyme was created by replacing the naturally occurring regulatory domains by two proteins that have a known interaction that can be inhibited by a small molecule[2]. This method gives the benefits of a small molecule in that it gives a dose dependent response and temporal control. Another benefit of this method is that it is general. These regulatory domains can be used as unnatural regulatory domains for a variety of proteins and can be activated by a single small molecule.

A. Design of Synthetically Regulated Protein Switch

Several factors needed to be met for the selection of the protein-protein interaction that would form the non-natural regulatory domains in our switch[2]. The interaction had to be genetically encodable and modular so that the switch could be easily engineered. For this method to be general, the inhibitor should only activate the switch, not interfere with cellular pathways. Also, a small molecule

inhibitor of the protein-protein interaction had to exist[2]. Not many small molecules exist that can disrupt the large interaction interface of two proteins. However, a small molecule has been developed that potently inhibits the interaction between two proteins: Bcl-Xl and Bad. Bcl-xL is a 21 kDa protein from the Bcl-2 family of proteins. It is largely alpha helical and these helicies come together to form a hydrophobic binding groove in which the pro-apoptotic BH3 family member Bad protein binds (**Figure 1-2A)**. It has been shown that when the peptide that binds into the hydrophobic binding groove is removed from the protein it still retains its low nanomolar binding affinity. The Bad peptide is utilized in the switch[2].

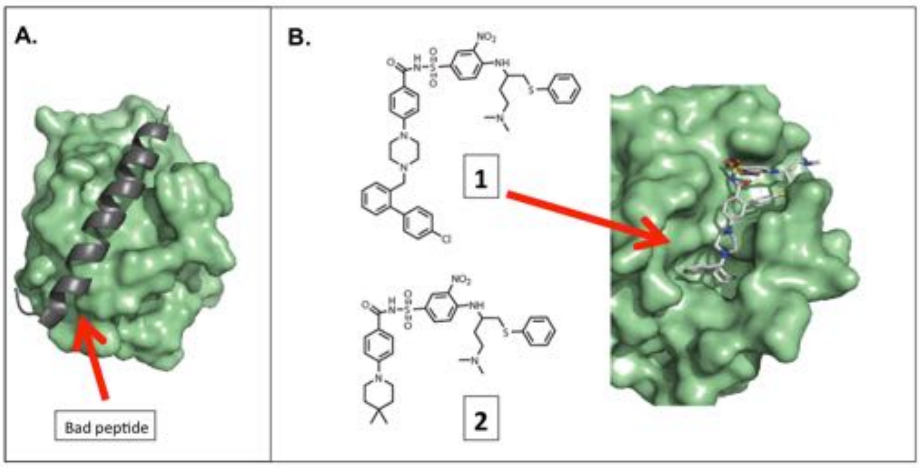

Figure 1-2: Interaction of BclXL and Bad and small molecule disruptors. **A.** Bcl-XL (green) bound to the Bad peptide (grey)**. B. 1.** Structure of ABT-737, **2.** Structure of ABT-385358 . The crystal structure shows ABT-385358 bound to **1.**

A number of small molecules that inhibit this interaction with low nanomolar potency (1nM) have been developed including ABT-737 and ABT-385358 (Figure 2)[3]. These inhibitors compete directly with the Bad peptide for the binding site of BclXL (**Figure 1-2B**). The ABT drugs were developed as anti-cancer therapy[3]. In healthy cells antiapoptotic Bcl-2 family proteins bind to proapoptotic BH3-family proteins, which inhibits apoptosis[4]. Upon initiation of apoptosis, cellular levels of

BH3 family members increase and the BH3 proteins are no longer sequestered by Bcl-2 family proteins, which cause apoptosis. However, in many types of cancerous cells, the Bcl-2 family proteins are over-expressed. This causes sequestration of the BH3 proteins and blocks apoptosis, leading to cancer. The ABT inhibitors were developed to disrupt the interaction of Bcl-2 family members with BH3 peptides so that apoptosis can occur[3]. However, these inhibitors were not successful in initiating apoptosis in all cell types.

There are five members of the Bcl-2 family: Bcl-xL, Bcl-W, Bcl-2, Mcl-1 and A1. ABT-737 A-385358 have low nano-molar dissociation constants (K_i<1nM) for Bcl-xL, Bcl-2, and Bcl-w but have minimal affinity for Mcl-1 and A1 (K_i>1μM)[5]. Mcl-1 and A-1 act redundantly to block apoptosis, so addition of the ABT inhibitors to cells does not cause cell death. To prove that these proteins were acting redundantly, knock-out studies of Mcl-1 and A-1 were preformed[6]. In the absence of the two proteins, cell death is observed upon addition of the ABT inhibitors.

B. Synthetically regulated protein switch can be used to modulate activity of Intersectin

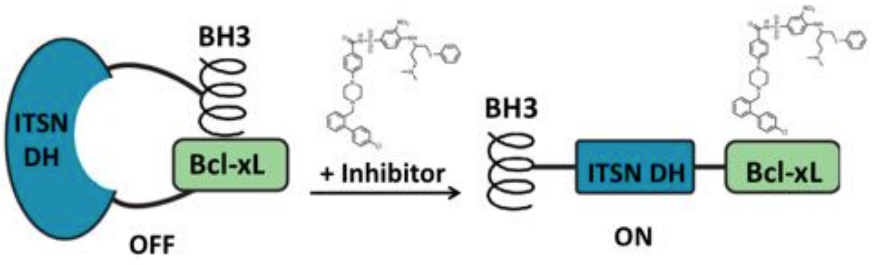

Figure 1-3: Regulation of Intersectin catalytic domain using Bcl-xL and Bad peptide as non-natural regulatory domains. In the presence of the small molecule inhibitor, the interaction between the regulatory domains is disrupted, which allows the catalytic domain to perform its function.

Previous work in our lab has demonstrated the utility of this switch[2]. The Guanine Nucleotide Exchange Factor (GEF) Intersectin was engineered into the switch (**Figure 1-3**). This Dbl family GEFs acts as an activator of Rho-family GTPase CDC-42 by catalyzing the exchange of GDP for GTP. Cdc42 is involved is cell migration and cytoskeltal rearrangement. When the switch is closed, the GEF is unable to activate Cdc-42. However, when the small molecule is added, the switch is opened allowing Intersectin to catalyze the exchange of GDP for GTP, which activates Cdc42. When Cdc42 is active, filipodia formation can be observed. To prove that this method can be used in cells, cells were transfected with the switchable intersectin as well as Cdc42. Compared to the control cells, which were not transfected with the Intersectin construct, cells treated with DMSO did not show a large increase in filipodia formation, indicating that when the switch is closed Intersectin is inactive[7]. However in the presence of the small molecule, the switch opens and Intersectin can activate Cdc42, leading to filipodia formation in 15minutes (**Figure 1-4**). This switch has also been shown to be general for other GEFs such as Tim and Tiam[7].

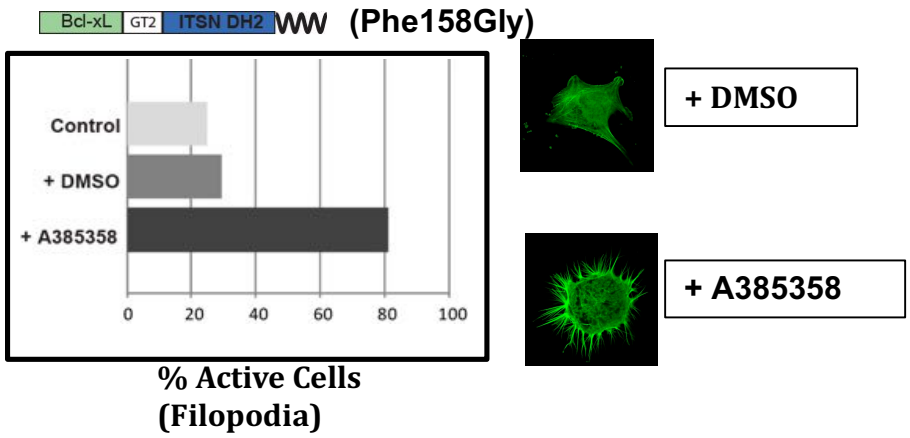

Figure 1-4. Formation of filipodia using the small molecule regulated switch to control Intersectin activity and therefore regulate CDC42. When cells are treated with DMSO there is a comparable amount of filipodia formation to the control cells that do not contain the regulated Intersectin. When cells are treated with the small molecule, filipodia formation increases to 80%, indicating that Intersectin is active and able to activate CDC42.

C. Cre Recombinase mechanism of action

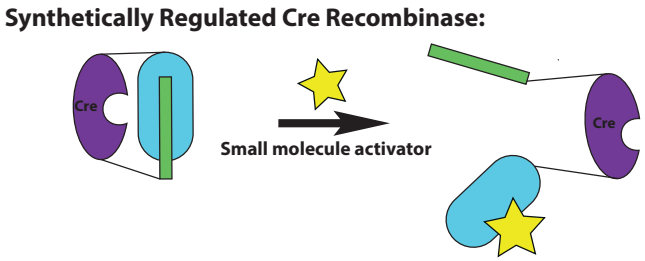

Figure 1-5: General Scheme for Synthetically Regulated Cre Recombinase. One Cre subunit is flanked by artificial regulatory domain BclXL and Bad peptide. In the presence of the small molecule activator, the interaction between the non-natural regulatory domain is disrupted, allowing Cre to catalyze recombinations.

Cre Recombinse (Causes Recombination) is a site-specific tyrosine recombinase from bacteriophage P1. The recoginition site of Cre is a short sequence of DNA called a LoxP site, which is not present in mammalian cells or vertabrates. Cre mediates recombination of genes flanked by loxP sites (called a "floxed" gene), resulting in excision, inversion or translocation depending on the

location and orientation of the loxP sites[8]. Cre has been shown to mediate recombination in a wide variety of cell types and also in animals. Cre is commonly used to facilitate conditional knock-in, knock-out and inversion studies is mammals[8].

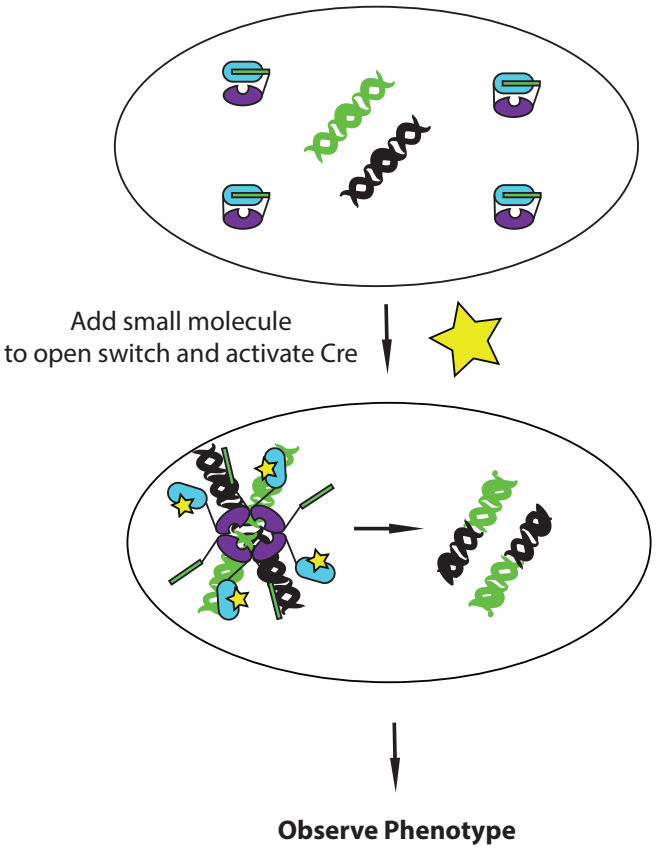

Figure 1-6: Cre recombinase autoinhibition in cells. Recombination occurs only after the addition of the small molecule inhibitor.

This synthetically regulated Cre recombinase system will be used to conditionally activate or inactivate gene expression in vivo in a tissue-specific manner with spatial and temporal control. In this system, one subunit of Cre recombinase is flanked by BclXL and the Bad peptide, which act as non-natural

regulatory domains (**Figure 1-5**). The recombinase remains inactive until the addition of the small molecule. Once the small molecule has been added, the interaction between the non-natural regulatory domains is disrupted and Cre is able to catalyze recombinations with temporal control. In this system, Cre is under the control of a non-toxic small molecule activator and can be used to mediate conditional recombination of any floxed sequence (**Figure 1-6**). Since Cre can be localized in a tissue specific manner, our system offers an effective way to study transgenes in animal models.

Four identical subunits of Cre come together to form the catalytically active tetramer[8]. Recombination takes place between two loxP sites, with two Cre subunits binding to each loxP site. The lox P site consists of two Recombinase Binding Elements (RBEs)[8] (**Figure 1-7A**). These RBEs are inverted repeats of each other. The area highlighted in yellow is the spacer region where cleavage and strand exchange occurs. **Figure 1-7B** shows the recombination mechanism of Cre recombinase. Two Cre subunits bind to each loxP site and two loxP sites associate to form a synaptic complex[8]. Catalysis is only able to occur when all four subunits of the recombinase come together. The cleavage reaction occurs in a stepwise manner, with only two recombinase subunits active at one time. The first two subunits cleave the loxP site in the spacer region with conserved Y324 to form a covalent 3'-phosphotyrosine intermediate and leaving behind a 5' hydroxyl. Intermolecular attack by the partner substrates 5'-hydroxyl group on the covalently linked phosphotyrosine completes exchange of the first pair of DNA strands and produces the Holliday Junction (HJ) intermediate. Isomerization of the HJ

intermediate results in activation of the second pair of recombinase subunits for cleavage, strand exchange and ligation on the complementary strands to form the recombined products[8].

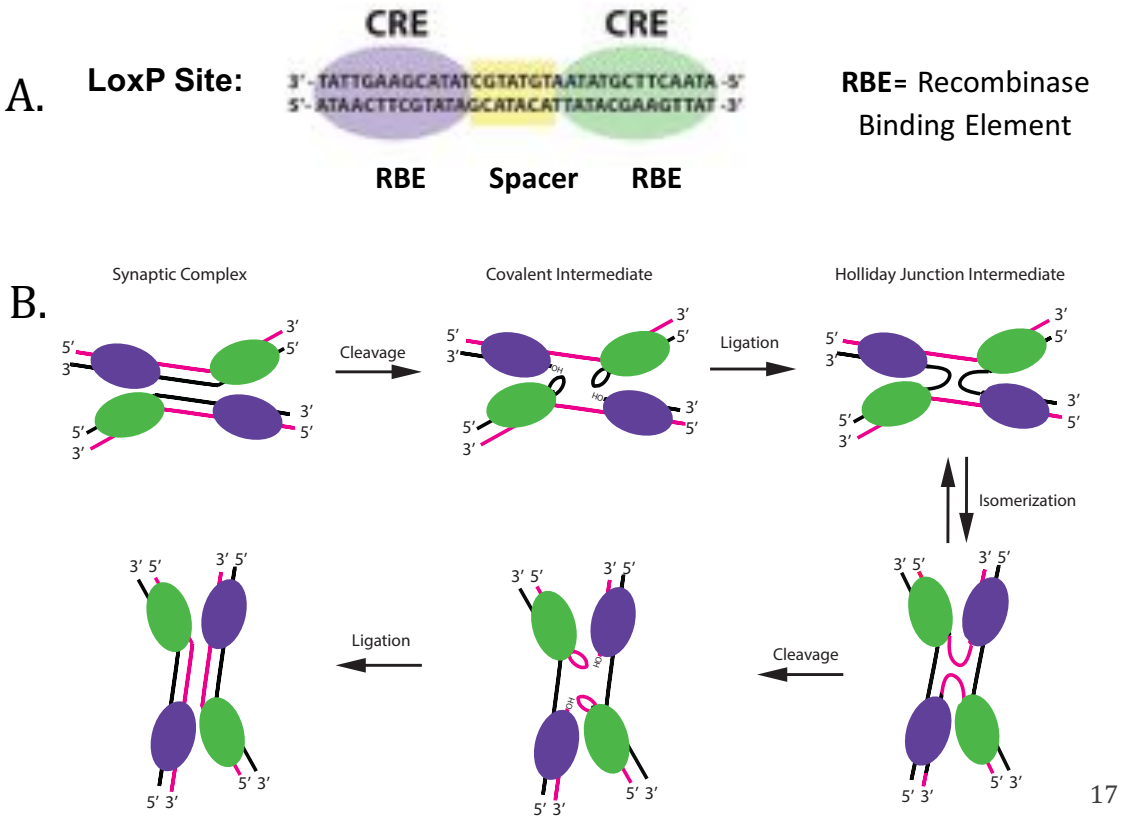

Figure 1-7: Mechanisim of Recombination (a) Diagram of LoxP binding site. Binding sites of Cre subunits are highlighted in purple and green. Space region is highlighted in yellow. (b) Mechanism of Cre Recombination.

The spacer region of the loxP site imparts directionality (**Figure 1-8A**). In order for strand exchange to occur, the loxP sites must have the same directionality. The orientation and location of the loxP sites give rise to three possible rearrangements of DNA[9] (**Figure 1-8B**). One type of recombination is inversion, which is a form of intramolecular recombination where the two loxP sites

are located on the same strand of DNA with opposite orientation to each other. After recombination occurs, the DNA flanked by the loxP sites is inverted. Intramolecular recombination where the loxP sites are both in the same orientation results in the excision of the region flanked between the two sites and circularization of the flanking regions. In translocation recombination, intermolecular recombination of sites located on two separate DNA molecules, will result in the integration of the two segments[9].

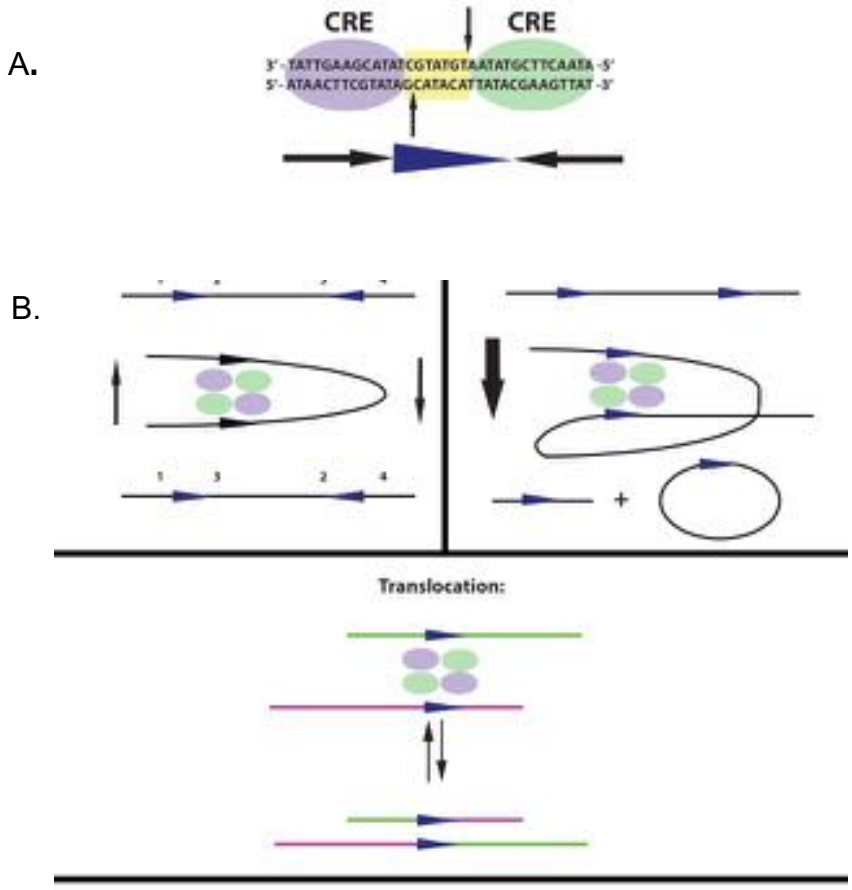

Figure 1-8: Types of recombination.
(a) Directionality of spacer region (yellow) shown by wedge shape. (b) Schematic of inversion, excision and translocation.

D. Current methods for controlling Cre Recombinase

The current method for controlling Cre Recominase is the Cre-ER method[10] (**Figure 1-9**). In this method, Cre is fused to an engineered steroid hormone receptor. The most commonly used receptor is a mutated Estrogen Receptor that no longer binds endogenous estradiol but retains affinity for the synthetic analog Tamoxifen. This fusion protein is called Cre-ER. When no Tamoxifen is present, the recombinase is sequestered to the cytoplasm by Hsp90. Since there is no DNA in the cytoplasm, Cre is not active. However, when Tamoxifen is added Hsp90 is displaced and the Cre-ER is translocated to the nucleus, which allows Cre to become active. The benefit of this system is that Cre becomes active in a ligand dependent manner[10].

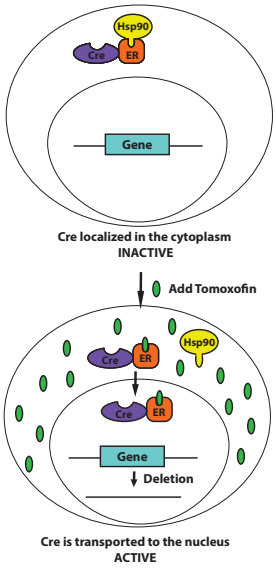

Figure 1-9: Cre-ER mechanism. Hsp-90 sequesters Cre-ER to the cytosol, where it is inactive. Upon addition of Tamoxifen, Cre-ER transloactes to the nucleus and becomes active.

Unfortunately, there are many drawbacks to this system. One issue is that the system is leaky, which means that some Cre is able to translocate to the nucleus even though Tamoxifen is not present[11]. Since only a few molecules of

Cre are required to catalyze a recombination reaction, this causes a high background. Another disadvantage is that the efficiency of the system is dependent on cell type, so each type of cell must be extensively tested before Cre-ER can be used[10]. Tamoxifen is dosed to the mice by oral gavage over a 5 days period. In many cases this drug causes the mice to become sick and leads to a significant number of deaths[12].

Recently, several other strategies have been developed to regulate Cre with spatial and temporal control. In the split Cre systems, Cre is fragmented and attached to two proteins capable of dimerization, usually FKBP/FRB which can be induced by addition of Rapamycin (diCre)[18]. These systems suffer from low activation and high toxicity caused by the chemical inducer of dimerization[19]. The split Cre approach has recently been expanded to photoactivatable dimerizers[20,21]. However, these systems frequently require exposure DNA damaging wavelengths for prolonged periods of time are less efficient in dense tissue and frequently requires insertion of a light emitting device in order to direct the light to the desired tissue [22,23].

II. Results and Discussion

A. Design of synthetically regulated Cre Recombinase

Ideally, the switchable Cre Recombinase would have low background when no drug is present and high activation once the drug has been added and would not require any specialized devices for activation. In order to find the ideally controlled Cre Recombinase the orientation of the switch components around one

subunit of Cre, the linkers connecting the Cre subunit to the components of the switch were varied. Also, the affinity of the Bad peptide for BclXL was varied.

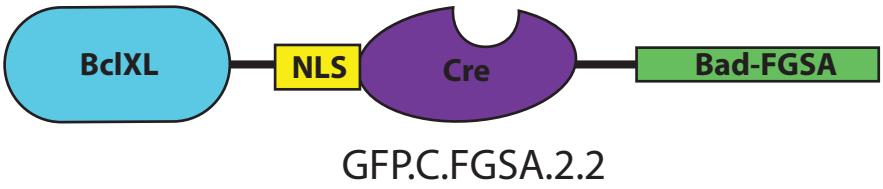

Figure 1-10: Sample switched Cre construct. Construct GFP.C.FGSA.2.2 contains a GFP, a C-terminal Bad peptide and BclXL and Bad are both linked to Cre by two GT repeats.

Each fusion protein consists of three core components (**Figure 1-10**): 1) one Cre recombinase subunit, 2) BclXL (residues 4-196) and 3) the Bad peptide that binds tightly to BclxL (residues 137-163 of the protein Bad) and 4) a nuclear localization signal (NLS). Variable flexible glycine-threonine repeat linkers $(GT)_X$ of varying sizes were used to fuse BclXL or the Bad Peptide to Cre. In addition, synthetic constructs were created with GFP tags so that the fusion proteins could be visualized. The constructs are named as follows: the location of the Bad peptide is indicated by N or C, followed by the mutation in the Bad peptide, the N- and C-terminal GT repeats are indicated by the numbers and constructs that contain a GFP tag are labeled as such. A panel of synthetic Cre fusion proteins was generated in order to find the optimal binding orientation of the artificial regulatory domains (**Table 1-1**).

N-Terminal Bad Peptide

N.WT.2.2	Bad WT-GT-NLS-CRE-GT-BclxI
N.FG.2.2	Bad FG-GT-NLS-CRE-GT-BclxI
N.WT.0.10	Bad WT-NLS-CRE-GT5-BclxI
N.FG.0.10	Bad FG-NLS-CRE-GT5-BclxI

C-Terminal Bad Peptide

WT Bad Peptide

C.WT.2.2	BclxI-GT-NLS-CRE-GT-Bad-WT
C.WT.2.6	BclxI-GT-NLS-CRE-(GT)3-Bad-WT
C.WT.2.10	BclxI-GT-NLS-Cre-(GT)5-Bad-WT

FS Bad Peptide

C.FS.2.6	BclxI-GT-NLS-CRE-(GT)3-Bad-FS

FG Bad Peptide

C.FG.2.2	BclxI-GT-NLS-CRE-GT-Bad-FG
C.FG.2.6	BclxI-GT-NLS-CRE-(GT)3-Bad-FG

FSSA Bad Peptide

C.FSSA.2.2	BclxI-GT-NLS-Cre-GT-Bad-FSSA
C.FSSA.2.6	BclxI-GT-NLS-Cre-(GT)3-Bad-FSSA

FGSA Bad Peptide

C.FGSA.2.0	BclXL-GT-NLS-Cre-Bad-FGSA
C.FGSA.2.2	BclxI-GT-NLS-Cre-GT-Bad-FGSA
C.FGSA.2.6	BclxI-GT-NLS-Cre-(GT)3-Bad -FGSA
C.FGSA.2.10	BclxI-GT-NLS-Cre-(GT)5-Bad-FGSA
C.FGSA.4.2	BclxI-(GT)2-NLS-Cre-GT-Bad-FGSA
C.FGSA.4.6	BclxI-(GT)2-NLS-Cre-(GT)3-Bad-FGSA

N-terminal GFP Tag

GFP.C.WT.2.2	GFP-BclxI-GT-NLS-Cre-GT-Bad-WT
GFP.C.FS.2.2	GFP-BclxI-GT-NLS-Cre-GT-Bad-FS
GFP.C.FG.2.2	GFP-BclxI-GT-NLS-Cre-GT-Bad-FG
GFP.C.FGSA.2.2	GFP-BclXL-GT-NLS-Cre-GT-Bad-FGSA
GFP.C.FGSA.2.0	GFP-BclXL-GT-NLS-Cre-Bad-FGSA

Table 1-1: Synthetically regulated Cre constructs. Organized by N- or C-terminal orientation of Bad peptide. Subgroup are organized by the mutation on the Bad peptide, with increasing linker lengths going down the group.

B. Determining optimal orientation for the switch

In order to determine if the synthetically controlled Cre constructs could be activated in cells by the small molecule, a convenient cellular assay was used. In this assay, HEK-293T reporter cells with an floxed stop codon preceding an RFP gene (**Figure 1-11A**). If no Cre is present, or if Cre is inactive, then the stop codon is not excised and no RFP is expressed. However, when active Cre is present, Cre catalyzes the excision of the stop codon, which results in the expression of RFP. The reporter cells were transfected with the synthetically regulated Cre construct, incubated for 24 hours, and then treated with either DMSO or ABT-385358 for 48

hours (**Figure 1-11B**). A rough quantitation was preformed in order to find the constructs with the lowest background RFP inversion and highest RFP induction after treatment with the drug.

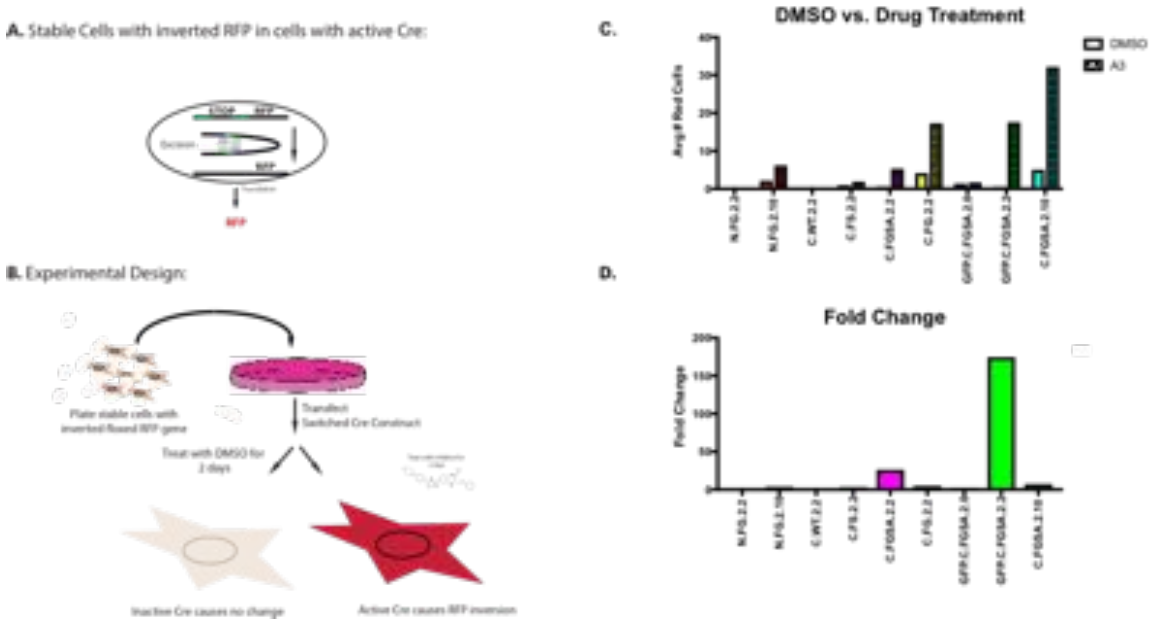

Figure 1-11: **Graphs of Representative Constructs** (a) Cell reporter scheme. Excision of stop codon by Cre Recombinase results in expression of RFP. (b)Scheme for RFP inversion assay: Reporter cells are transfected with construct, then treated with either DMSO or ABT-385358 for 48 hours. Cells are imaged using fluorescent microscopy. (b) Comparison of constructs. Top graph shows total number of red cells in DMSO treated cells vs. drug treated cells. Bottom graph shows fold change =(#red cells in drug treated sample/ # of red cells in DMSO treated sample.) Constructs with a GFP tag and with N- and C-terminal linkers that contained two GT repeats were tested further.

Constructs with an N-terminal Bad peptide (N.FG.2.2 and N.FG.2.10) showed little or no ability to be activated with the small molecule inhibitor, while C-terminal Bad peptide constructs showed ability to be activated with the small molecule (**Figure 1-11C and D**). The constructs with N- and C-terminal linkers that contained two GT repeats and an FGSA mutation in the bad peptide (C.FGSA.2.2., GFP.C.FGSA.2.2) showed the lowest number of red cells in the DMSO treated control and the highest fold activation in the presence of drug. Lengthening the

linker in GFP.C.FGSA.2.10 caused a higher background, although the activation was increased. There was also an unexpected, but dramatically higher activation with the addition of a N-terminal GFP tag.

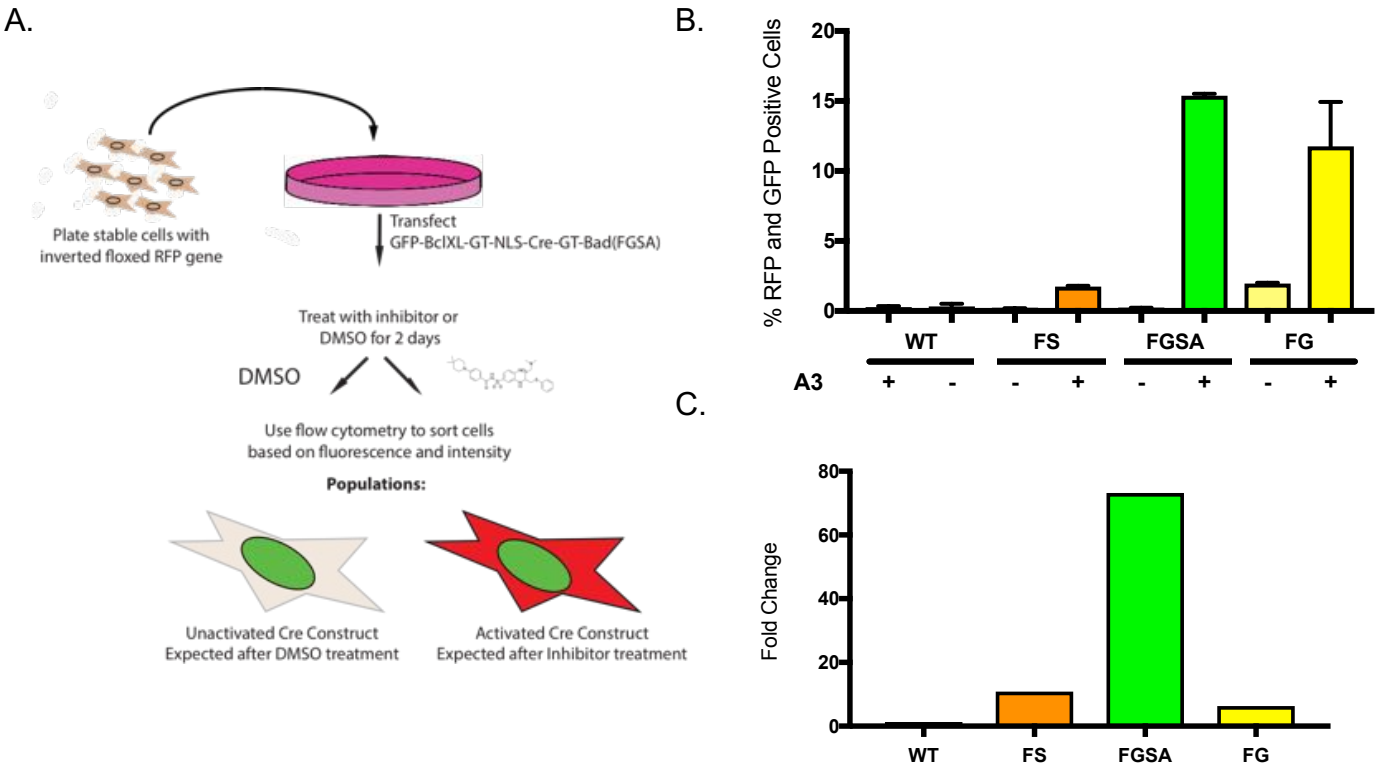

Figure 1-12: Flow cytometry experimental results. A. FACS experiment. RFP reporter cells were transfected with GFP-tagged constructs. Cells were treated with either DMSO or ABT-385358. DMSO treated cells should be GFP positive. ABT-385358 treated cells should be GFP and RFP positive B. Percentage of double positive cells after DMSO treatment(-) or treatment with A3(+).HEK293T reporter cells were transfected with respective DNA for 24 hours then treated with either DMSO or 20uM A3 for 48 hours. Cells were washed with PBS, trypsinized, resuspended in PBS with 5% FBS and sorted by FACS. C. Fold activation of constructs: Fold change = number of double positive cells after treatment with drug/ number of double positive cells after treatment with DMSO.

Flow cytometry was used to quantitavely compare the level of RFP reporter expression in cells transfected with the best preforming constructs from the previous experiments, which contained a GFP tag for easy visualization and two flexible residues at the N- and C-termini, in the presence of DMSO or ABT-385358.

Cells were sorted by fluorescent dye (RFP reporter, GFP-tagged switched cre construct) and fluorescent intensity (**Figure 1-12A)**. Cells that were positive for both GFP and RFP were compared for the drug treated and DMSO treated cells. The optimal switched Cre would have low activation in the presence of DMSO, but high activation in the presence of ABT-385358, which we hypothesized could be further optimized by tuning the affinity of the Bad peptide for BclXL. It is difficult to disrupt the intramolecular reaction of BclXL and the Bad peptide with an intermolecular inhibitor of similar affinity[2], so a panel of mutants that reduce the affinity of the Bad peptide for BclXL was tested (**Figure 1-12 B and C**). Phe158Ser and Phe158Gly have reduced binding affinities for BclXL of 33-fold and 75-fold respectively. Ser155 has been identified as a potential substrate for phosphorylation, so the Ser155Ala was utilized to ensure that only small molecule binding disrupts the interaction between the artificial regulatory domains. As expected, GFP.C.WT.2.2 showed low background recombination with no activation, GFP.C.FS.2.2 showed low background recombination (0.1%), but only 3.8 fold activation. The GFP.C.FG.2.2 mutation showed the highest background recombination at 1.86%, which is consistent with the reduced binding affinity of Phe158Gly for BclXL compared to WT, which rendered it useless although it showed a high activation. Construct GFP.C.FGSA.2.2 was found to have the optimal binding strength with only 0.1% background recombination. This is of great importance because it only takes a small number of Cre molecules to catalyze recombination. It also showed a 75-fold activation upon addition of the drug. This

construct gives the desired low background and high activation that is ideal for a small molecule regulated Cre.

C. Determining the mechanism of autoinhibition

Our cellular data proved that the synthetically regulated Cre recombinase was working well, but the mechanism of autoinhibiton was unknown. First, the localization of construct GFP.C.FGSA.2.2 was determined using confocal microscopy. Cells were plated on coverslips, transfected with construct GFP.C.FGSA.2.2, fixed and stained with DAPI nuclear stain (Figure 1-13). Overlay with the nuclear stain shows that the GFP.C.FGSA.2.2 construct is nuclear with and without drug treatment, indicating that inhibition of catalysis is not due to sequestration in the cytosol.

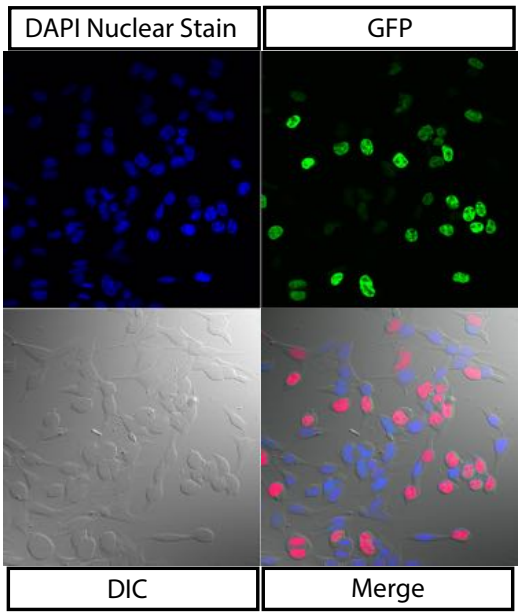

Figure 1-13: GFP.C.FGSA.2.2 is Localized in the Nucleus. Cells were transfected with GFP.C.FGSA.2.2 for 24 hours then treated with ABT-385358 for 48 hours. Cells were fixed, stained with DAPI and imaged using confocal microscopy.

Modeling studies in our lab indicated that the mode of autoinhibition of the synthetically regulated Cre Recombinase was due to blocking formation of the synaptic complex. In the proposed model, Cre subunits are still able to bind to the lox P site, but two loxP sites cannot come together to form the synaptic complex due to steric hindrance caused by the interaction of BclXL and the Bad peptide as seen in (**Figure 1-14**).

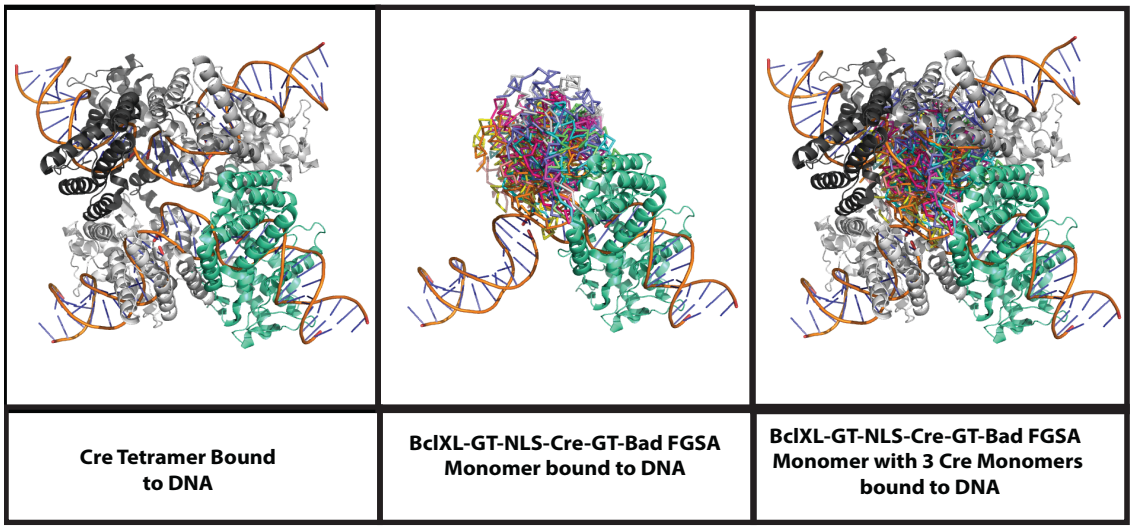

Figure 1-14: Switched Cre Modeling. Modeling shows that the switch blocks formation of the synaptic complex and therefore catalysis of Cre, but still allows Cre to bind DNA.

In order to confirm the model, an Electrophoretic Mobility Shift Assay (EMSA) of *in vitro* binding studies was preformed[13]. This assay tests the ability of the Cre subunits to bind DNA and form the synaptic complex. Biotinylated double stranded DNA containing one loxP site was incubated with Cre WT, construct GFP.C.FGSA.2.2 with DMSO or construct GFP.C.FGSA.2.2 with ABT-385358 (**Figure 1-15**). We were gratified to find that when no drug is present, construct GFP.C.FGSA.2.2 is able to bind DNA as a monomer and as a dimer, however no

tetrameric synaptic complex was formed. However, when ABT-385358 was added, a band for the tetrameric complex was observed. This confirms our modeling results that the artificial regulatory domains block formation of the tetrameric synaptic complex, but still allow the Cre subunits to bind DNA.

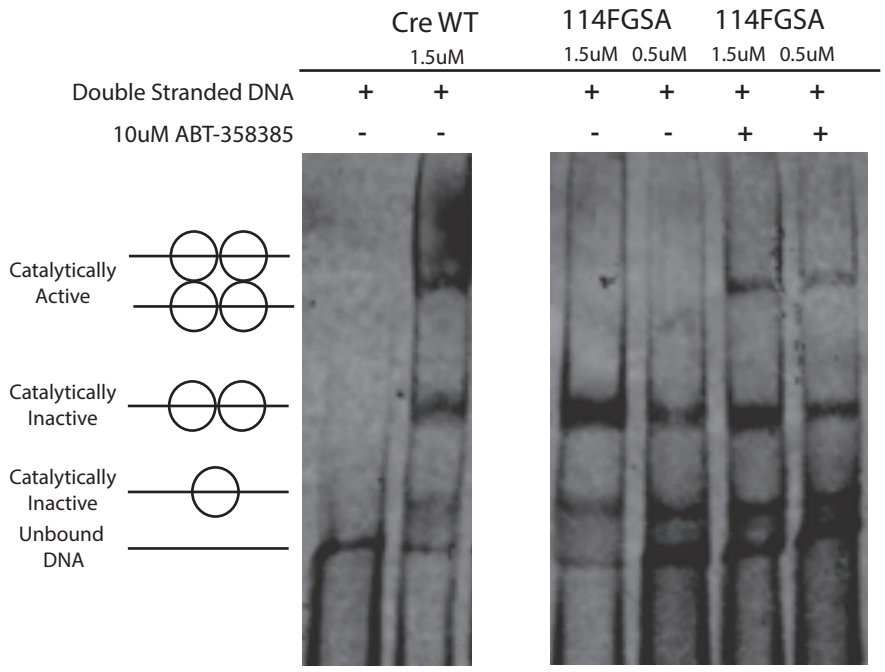

Figure 1-15: EMSA Assay shows Cre subunits bound to DNA. WT Cre shows formation of the tetrameric synaptic complex. Construct GFP.C.FGSA.2.2 shows no tetrameric synaptic complex, however once ABT-385358 is added, the synaptic complex can be observed. This indicates that autoinhibition is a result of blocking formation of the synaptic complex.

D. Initial studies in mice

Our ultimate goal is to use the synthetically regulated Cre Recombinase in animals. Abbot initially developed the small molecule activator ABT-385358 as an anti-cancer therapy, however it was found that it does not cause apoptosis[6,12]. ABT-385358 binds with subnanomolar potency to three out of five family members of the Bcl-2 family: BclXL, Bcl2 and BclW, but it does not bind to Mcl-1 or A-1.

These two anti-apoptotic proteins act redundantly to rescue the cell from apoptosis. Animal studies have been preformed ABT-385358. In this study it was found that the compound was well tolerated by the mice at a dose of 75mg/kg/day[12]. In order to be certain that the drug was well tolerated, we did a week long trial of injections at 75mg/kg/day in two mice and found that they survived with no ill effects (**Figure 1-16**).

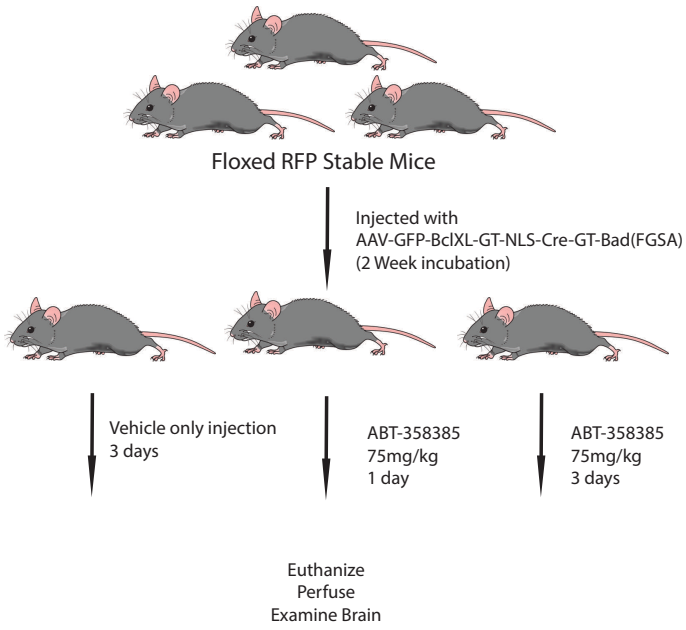

Figure 1-16: Experimental scheme for mouse studies. Transgenic mice are injected with virus containing the synthetically regulated Cre construct GFP.C.FGSA.2.2. Then mice are treated with either vehicle or ABT-385358. The mice are then euthanized, perfused and the brains are examined using fluorescent microscopy.

Our first experiment was to test if synthetically regulated Cre construct GFP.C.FGSA.2.2 could be activated by the small molecule to invert an RFP gene in mice neurons . Three transgenic reporter mice with the inverted RFP gene integrated into neurons in the striatum were injected with a virus encoding for the

synthetically regulated Cre construct GFP.C.FGSA.2.2. After two weeks one mouse received a control injection of the delivery vehicle for three days, the other two mice received injections of ABT-385358 at 75mg/kg/day, one mouse received injections for one day, the other received injections for three days. The mice were euthanized, perfused, and their brains were extracted and examined by fluorescent microscopy. Since the synthetically regulated Cre construct contains a GFP tag, we were able to visualize the cells that expressed the Cre construct.

Unfortunately, we did not observe an increase in red cells in the drug treated mice compared to the vehicle treated mouse. We believe that his is because the compound did not cross the Blood Brain Barrier (BBB.) Since ABT-385358 has a molecular weight of 639 daltons, this is not unexpected as it violates Lipinski's rules. Although we were unable to see activation of Cre, we did observe a very low number of red cells in the neurons of the mice (**Figure 1-16**). This shows that the synthetically regulated Cre recombinase is tightly auto-inhibited and appears to have a lower background than the Cre-ER system. This is an important feature, since it only takes a small number of Cre molecules to catalyze recombination. Another benefit of our system over that of Cre-ER is that the small molecule activator is well tolerated in mice, with minimal side effects, unlike the toxic and potentially fatal effects of Tamoxifen[12].

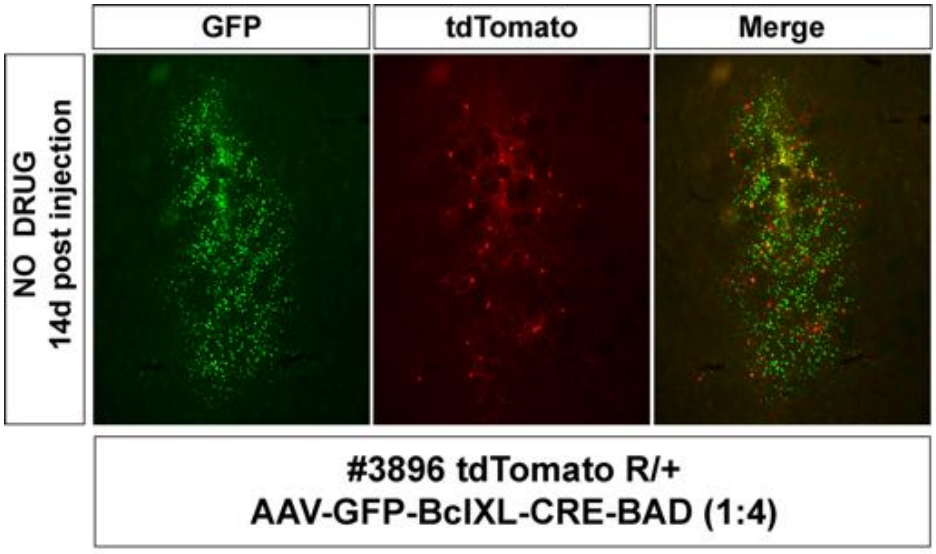

Figure 1-17: Representative image of treated mouse brain. Drug does not cross the blood brain barrier, however it is apparent that the synthetically regulated cre construct is tightly autoregulated and shows a minimal number of background red cells.

III. Conclusion

In conclusion, our results demonstrate that we discovered a well-controlled synthetically regulated Cre construct that is tightly auto-inhibited, but has a high activation in mammalian cells. We were able to determine the method of inhibition through biochemical studies. We found that the construct is localized to the nucleus and is therefore fundamentally different than other chemically induced Cre systems. Our switch blocks the ability of Cre to form the synaptic complex necessary to cause recombination, however the switched subunits are still able to bind DNA as monomers and as dimers. We have also shown that the small molecule activator of Cre ABT-385358 is well tolerated in mice, although it does not appear to cross the BBB. This is an improvement over current systems in which toxic doses of drug or invasive methods of drug delivery are required. This

synthetically regulated Cre construct is tightly auto-inhibited and shows great promise for tissue specific applications, such as the liver or muscle tissue. Current investigations are underway to determine the rate at which the switched-Cre edits DNA. In combination with tissue directed localization of Cre Recombinase, this system offers high spatial and temporal control over recombination in mammalian cells.

IV. Materials and Methods

A. Cloning of switched Cre constructs:

Bcl-xL (residues 2-215; human), Cre Recombinase (residues 2-341; P1 bacteriophage) and the Bad peptide were subcloned into pcDNA3.2 V5 plasmid or for constructs with an N-terminal GFP, the Lic-GFP plasmid, both mammalian expression vectors using Gibson Assembly (NEB, product number E2611L).

B. Initial RFP Inversion Assay in Reporter Cells

HEK293T reporter cells stably transfected with inverted floxed RFP were grown in a 12 well plate. 20ng of DNA was transfected per well using the calcium phosphate method of transfection. The cells were incubated for 24 hours and then treated with 10uM ABT-385358 (0.1% DMSO final) or with 0.1% DMSO for 48 hours. Cells were examined using fluorescent microscopy and quantitated by counting the average number of red cells per 10 fields of view. Data are presented

as the ratio of the number of red cells in the presence of ABT-385358 divided by the number of red cells in the presence of DMSO.

A. Quantitation of RFP Expression using Flow Cytometry

HEK293T cells stably transfected with inverted floxed RFP were grown in a 6 well plate. 1μg of DNA was transfected using X-tremeGeneHP transfection reagent (Roche.)The cells were transfected for 24 hours and then treated with 10uM ABT-385358 (0.1% DMSO final) or with 0.1% DMSO for 48 hours. The cells were washed twice with PBS and resuspended to 2 x 10^8 cells/mL in PBS, 2% FBS, 10μg/mL DNaseI. Cells were counted using the LSRII Flow Cytometer, 10,000 GFP positive events were collected for each data point. Data was quantitated using FloJo.

C. Localization of synthetically regulated Cre Construct GFP.C.FGSA.2.2

HEK293T cells stably transfected with inverted floxed RFP were grown in a 12-well plate on coverslips. 500ng of DNA was transfected using X-tremeGeneHP transfection reagent (Roche.) The cells were incubated with for 24 hours and then treated with 10uM ABT-385358 (0.1% DMSO final) or with 0.1% DMSO for 48 hours. The cells were washed twice with PBS, fixed with 4% paraformaldehyde, stained with DAPI and mounted using fluoromount. Cells were imaged using a Zeiss Confocal Microscope.

D. Purification of Cre Recombinase

Cre Recombinase (residues 2-341, P1 bacteriophage) and Synthetically regulated Cre Recombinase construct GFP.C.FGSA.2.2 were subcloned into pET-28a, a bacterial expression vector containing an N-terminal polyhistidine tag, using Gibson Assembly Cloning (NEB.) Synthetically regulated Cre protein was expressed in *E. coli* BL21 cells by inoculating 250 mL of LB broth containing ampicillin (100 µg/mL). Cultures were grown at 37°C to an OD600 of 0.6-0.8 and induced at 25°C for 4 h with 1 mM IPTG. To purify the protein, bacterial pellets were re-suspended in PBS buffer, pH 7.4 containing PMSF (100 µg/mL), followed by sonication and centrifugation at 4°C to clear the lysate. The cleared lysate was purified using NiNTA agarose (Qiagen) by rotating at 4°C for 1 hour. Subsequently, the resin was washed 4x and the protein eluted with 300 mM imidizole. All Bcl-xL mutants were expressed and purified using a similar procedure.

E. EMSA Assay

The probe for electrophoretic mobility shift assays was a 64 bp duplex containing the *loxP* site flanked by 15bp G·C-rich segments and labled with biotin at the 3' end of the top strand. 500nM or 1,500nM of Cre WT, GFP.C.FGSA.2.2 + 0.1% final DMSO, or GFP.C.FGSA.2.2 + 10uM ABT-385358 were added to 0.2nM biotinylated dsDNA substrate in binding buffer (10mM Tris pH 7.4, 150mM NaCl, 5% glycerol, 50ng/uL Poly (dI·dC), 0.2mg/mL BSA) for 20 minutes at 20°C. Binding reactions were electrophoresed on a 5% non-denaturing polyacrylamide gel in 0.5x TBE that was pre-run at 100V for 1 hour at 4°C prior to loading. The gel was run

at 100V for 1 hour at 4°C. The gel was transferred to a nylon membrane, which was presoaked in 0.5x TBE for 10 minutes, by transferring at 100V for 60minutes at 4°C. The membrane was dried and crosslinked by a 254nm hand held UV light at a distance of 5cm for 10minutes. The membrane was blocked in Odyssey Blocking Buffer (Li-Cor Blocking Buffer) for 10 minutes, then labled with IRDyeCW Streptavidin at a 1:5,000 dilution. The blot was then imaged on a Li-Cor Imager.

II. Chapter 2: A Chemical-Genetic Strategy for the Investigation of Kinase Non-Catalytic Function using Covalent Conformation-Selective Inhibitors

I. Introduction

Through X-ray crystallography of kinases in complex with various small molecule inhibitors, three structurally distinct inhibitor stabilized kinase conformations have been found across many kinase families (Berman et al, 2000). The most predominately inhibitor stabilized kinase conformation is the active conformation, known as Type I. This conformation has an active site that is competent for phosphate transfer with the salt bridge between Glu310 and Lys298 intact. In contrast, there is a subset of two inhibitor stabilized catalytically inactive kinases that have been crystallized. In Type IIA inhibitor bound kinases, the catalytic DFG motif is flipped 180°, which leads to loss of kinase activity (Ranjitkar et al, 2010; Ranjitkar et al, 2014; Seeliger et al, 2009; Okram et al, 2006). In the Type IIB stabilized conformation, the alpha c-helix loop is rotated such that the important salt bridge between Glu310 and Lys298 is disrupted. (Muller et al, 2015; Palmieri and Rastelli, 2013; Georghiou et al, 2012). (**Figure 2-1)**

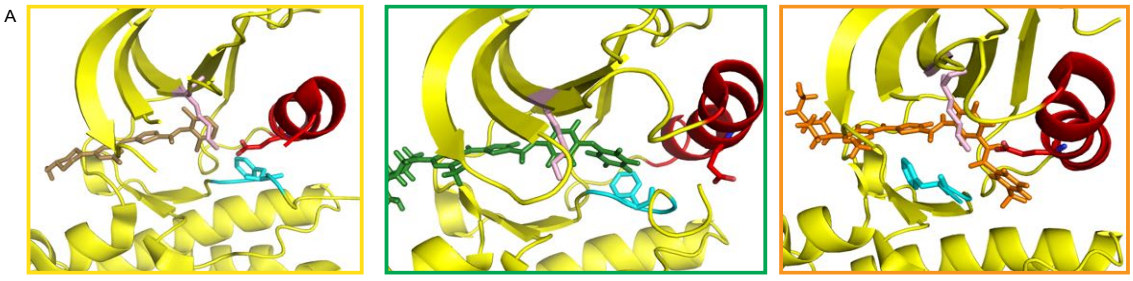

Figure 2-1 Crystal structures of three structurally distinct inhibitor stabilized Src catalytic domains.

From left to right: active/Type I-stabilized (yellow box, PDB: 3G5D), aC helix-out-stabilized (green box, PDB: 4YBK), and DFG-out-stabilized (orange box, PDB: 4YBJ). In each ATP-binding site, the aC helix is shown in red, the DFG motif is colored cyan, and the catalytic Lys is colored pale pink.

Since the active site of kinases and the regulatory domains show a high degree of allosteric coupling, stabilizing a particular active site conformation also has an impact on non-catalytic activity of the kinases. There are many recent studies, in our lab and by others, that link inhibition with DFG-in, DFG-out and αC helix out stabilizing inhibitors of kinases to a phenotypic effect. For example, it has been shown that ATP binding site conformation modulates dimerization of the serine/threonine kinase B-raf (Hatzivassiliou et. al 2010; Poulikakos et all 2014; Shepherd et. al. 2010; Heidorn et. al. 2010; Brennan et. al. 2014). When bound to Type I and Type IIA inhibitors, B-Raf dimerization increases dimerization and therefore downstream MAPK signaling. Interestingly, stabilization of B-Raf with a Type IIB inhibitor only shows weak dimerization and does not translocate to the membrane, which is a requirement for extended Raf activation. The divergent effects of stabilizing the kinase conformation on sites distal to the inhibitor binding site has led to speculation that the ATP binding site conformation can allosterically control global kinase conformation, which impacts signaling through phosphorylation state, cellular localization and inter-molecular binding partners. There are examples in the literature of catalytically inactive kinases playing a role in signaling networks. (Chen et al., 2006; Galan-Moya et al., 2008.) Conformationally selective inhibitors can be used as tools to probe the non-catalytic functions of protein kinases to investigate their role in signaling networks.

One large hurdle for studying non-catalytic function of protein kinases is the lack of selective Type I, Type IIA and Type IIB inhibitors for most kinases. Kinases share a large amount of structural homology that makes targeting one kinase extremely challenging (Anastassiadis et al., 2011). There have been several strategies developed to overcome the selectivity issue, including the "Bumped Hole" approach pioneered by Kevin Shokat. In this method, the inhibitor is made larger and a compensating mutation at the gatekeeper residue of the kinase to a smaller Gly or Ala is made to accommodate the bulkier inhibitor (Bishop et al., 2000). Mutating the gatekeeper residue has been shown to render kinases catalytically inactive and can potentially alter the allosteric coupling between the active site conformation and the regulatory domains (Azam et al., 2008; Garske et al., 2011). Another issue is that these inhibitors have only been made for Type I inhibitors.

In order to study the non-catalytic function of protein kinases, classes of inhibitors that are selective for a single kinase and allow the kinase to retain catalytic function are required. We adapted a method developed by the Taunton Lab to develop conformation-selective inhibitors that are specific for drug-sensitized SFKs, (Serafimova et al., 2012; Miller et al, 2013). In this method, a conserved N-lobe Val residue is mutated to a Cys that can create a reversible covalent bond with various Type I and Type II inhibitors. This chemical genetic method is attractive because it allows for potent, reversible and selective inhibition of a kinase of interest. In this work, we describe how this strategy can be used to

probe the non-catalytic roles of protein kinases in localization and inter-molecular interactions in cells.

II. Results and Discussion

Our lab has generated conformationally selective reversible covalent inhibitors of Src kinase. Using a strategy developed by the Tauton lab, where a non-catalytic residue is mutated to a cysteine, which reacts with an electron deficient olefin containing inhibitor. Reversible covalent inhibitors have advantages over traditional irreversible covalent inhibitors. Compared to irreversible covalent inhibitors, the off target effects of reversible covalent inhibitors is minimized since covalent adducts with off target proteins are reversible (Bradshaw et al, 2015). Another advantage is that the residence time of these reversible covalent inhibitors can be tuned, whereas irreversible covalent inhibitors build up over time (Bradshaw et al, 2015).

A. Characterization of potent and selective Type I and Type II inhibitors

The utility of this system was originally demonstrated using the kinase RSK2, which has a non-catalytic Cys in the ATP binding site of the C-terminal Domain (CTD). (Serafimova et al., 2012; Miller et al, 2013). This Cys is conserved in only 11 kinases, which allowed for high selectivity. To expand further on this system, we created a cysteine mutant in the binding pockets of Src, Hck, Abl, Erk2, EphA2 and Pak1 by mutating a well conserved Val residue that aligns with the Cys of Rsk2 (**Figure 2-2B**). For the remainder of this work, these analog sensitive mutants will be referred to as Src^{AS}, Hck^{AS}, Abl^{AS}, $Erk2^{AS}$, $EphA2^{AS}$, and $Pak1^{AS}$.

Each of these kinases had previously reported non-catalytic function, which we hoped to modulate with our conformationally selective inhibitors.

A panel of conformationally selective inhibitors was created by modifying DFG-in, DFG-out and αC helix-out stabilizing pyrrolopyrimidine inhibitors with a cyanoacrylamide Michael acceptor moiety (**Figure 2-2C**). In these modified conformationally selective inhibitors, the reactive β-carbon of the cyanoacrylamide is pointing directly towards the reactive Cys of the ATP binding site.

In order to determine the selectivity of these inhibitors for the Analog Sensitive (AS) mutant over the WT kinases, activity assays were preformed resulting in inhibitors **1-4**. Inhibitor **1** is an electrophilic derivative of the DFG-in stabilizing inhibitor PP2, which does not make contacts with the DFG-motif or the αC-helix (Krishnamurty et al., 2012; Miller et al. 2013). Inhibitor **2** is an electrophilic analog of the αChelix-out stabilizing inhibitor, with a bulky substituent at the C3 position that has been shown to force the αC-helix into an out position. Inhibitors **3** and **4** are predicted to stabilize the DFG-out conformation, where the αC helix is in the in position and electrostatic contacts are made with Glu310 and the DFG pocket is occupied by a bulky substituent. **Figure 2-2C** shows example IC_{50} curves for $Hck3D^{AS}$, which contains the SH2, SH3 and analog sensitized catalytic domain Hck of shown by the colored lines, and HckWT in black lines that lacks the analog sensitizing mutation. The electrophilic analogs show a greater than 1,000 fold selectivity for the analog sensitized mutants over the WT, when the IC_{50} is measured at 1mM ATP (**Figure 2-2D**). The only exceptions were Pak1, which still needs to be compared to the WT and $Erk2^{AS}$, which was not inhibited by **3** or **4**. K_i

values were calculated using the Cheng-Prusoff equation for competitive inhibition as well as the determined K_m for ATP.

A

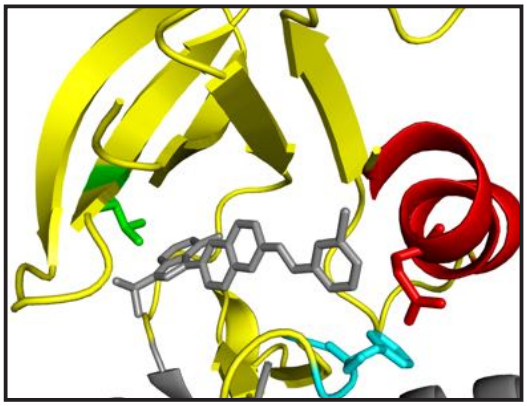

B

```
RSK2CTD FTDGYEVKEDIGVGSYSVCKRCIHKAT
Abl     ERTDITMKHKLGGGQYGEVYEGVWKKY
Hck     PRESLKLEKKLGAGQFGEVWMATYNKH
Src     PRESLRLEVKLGQGCFGEVWMGTWNGT
Erk2    VGPRYTNLSYIGEGAYGMVCSAYDNVN
Pak1    PKKKYTRFEKIGQGASGTVYTAMDVAT
```

C

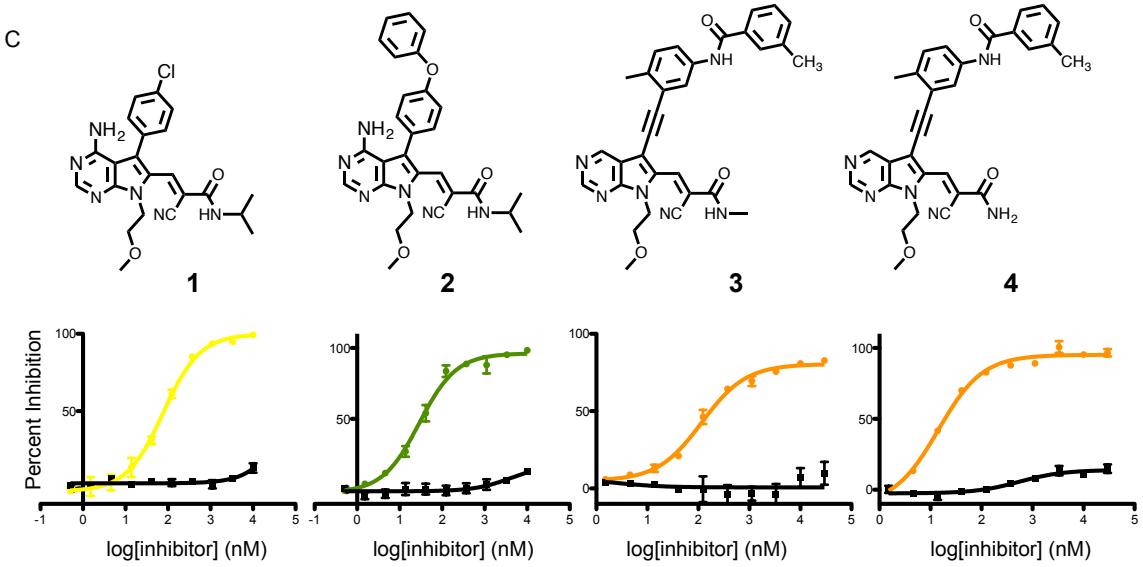

D

	AS		WT	AS		WT	AS		WT	AS		WT
	IC_{50}	K_i	IC_{50}	IC_{50}	K_i	IC_{50}	IC_{50}	K_i	IC_{50}	IC_{50}	K_i	IC_{50}
Abl	150±30	15 ± 6	>20000	200±40	22 ± 8	>20000	780±30	80 ± 15	>30000	26 ± 6	3 ± 1	>30000
Hck	77 ± 2	5.9±0.9	>20000	30 ± 6	2.3± 0.8	>20000	120±10	9 ± 2	>30000	14 ± 1†	NC	>30000
Src	26 ± 2	1.9±0.2	>30000	28 ± 3	2.1±0.2	>30000	44 ± 7	3.3±0.5	>30000	34 ± 3	2.5±0.2	>30000
Erk2*	ND	84 ± 6	>20000	6.3±0.7	3.4±0.2†	>20000	>30000	NC	>30000	ND	1200±120	ND
Pak1*	ND	ND	ND	ND	30	ND	ND	40	ND	ND	20	ND
EphA2*	18 ± 3	0.28±0.04	>30000	260±20	3.6±0.3	>30000	49 ± 4	0.71±0.05	1000±100	32 ± 2	0.43±0.03	840±50

Figure 2- 2: Hck, Abl, Src, Erk2, EphA2, and Pak1 can be sensitized to inhibition by covalent, conformation-selective inhibitors via non-catalytic active site Cys mutation

A. Crystal structure of the Src kinase domain ATP-binding site (PDB: 4DGG) bound to αC helix-out-stabilizing inhibitor RM 1-176 (grey). The αC helix is colored red and rotated such that Glu310 is no longer coordinated with Lys295 (αC helix-out, Type II). The DFG-motif on the activation loop (cyan) is in the "DFG-in" conformation. The Val residue to be mutated to Cys is shown in green. **B**. Sequence alignment of the kinases investigated in this study (Abl, Hck, Src, Erk2, EphA2, and Pak1) with the RSK2 C-terminal Domain (CTD). The RSK2 CTD Cys residue which can be targeted pharmacologically by reversible-covalent inhibitors is a conserved Val in most other kinases (green). **C**. Conformation-selective inhibitor structures and IC_{50} curves showing the potency of each inhibitor for the cysteine mutant Hck3D construct ($Hck3D^{AS}$) (colored) versus wild-type Hck3D (black). Yellow denotes that **1** stabilizes a Type I/active ATP-binding site, green denotes that **2** stabilizes a Type II/αC helix-out ATP-binding site, and orange denotes that **3** and **4** stabilize a Type II/DFG-out ATP-binding site conformation. This color scheme is maintained throughout the paper. **D**. Table displaying the IC_{50} and K_i values of **1**-**4** for each AS kinase construct tested and IC_{50} values for each WT kinase construct tested. All IC_{50} values were determined at 1mM ATP. K_i values were calculated via the Cheng-Prusoff equation assuming competitive inhibition. † Signifies that IC_{50} is too close to enzyme concentration used in the assay to be certain of true potency.

In order to determine the selectivity of the analog sensitive mutant kinase and Michael acceptor inhibitor pairs, a SILAC proteomics experiment was preformed (Golkowski et al., 2014). In this experiment, HEK293T cells are grown in the presence of heavy (C-13 labeled) media or light (C-12 labeled) media. The cells grown in the heavy media were exposed to 50μM of **1**-**4**, while cells grown in the light media were treated with DMSO (**Figure 2-3A**). The cells are washed, lysed and exposed to KinoBeads. KinoBeads contain a proprietary mixture of inhibitors that have been shown to bind to over 330 kinases (Golkowski et al., 2014). In this experiment, the kinases that are strongly inhibited by **1-4** are unable to bind to the KinoBeads and are washed away. The kinases remaining on the beads are digested and the peptides are quantitated by MS/MS. 220 kinases were quantitated in this assay. The quantitation of the peptides in the two conditions are

compared and the peptides that are depleted in the drug treatment compared to the DMSO control are from kinases that strongly interact with the inhibitor. These data were mapped by percent competition on a kinase dendrogram, where large circles indicate kinases that were strongly depleted (**Figure 2-3 B-E)**.

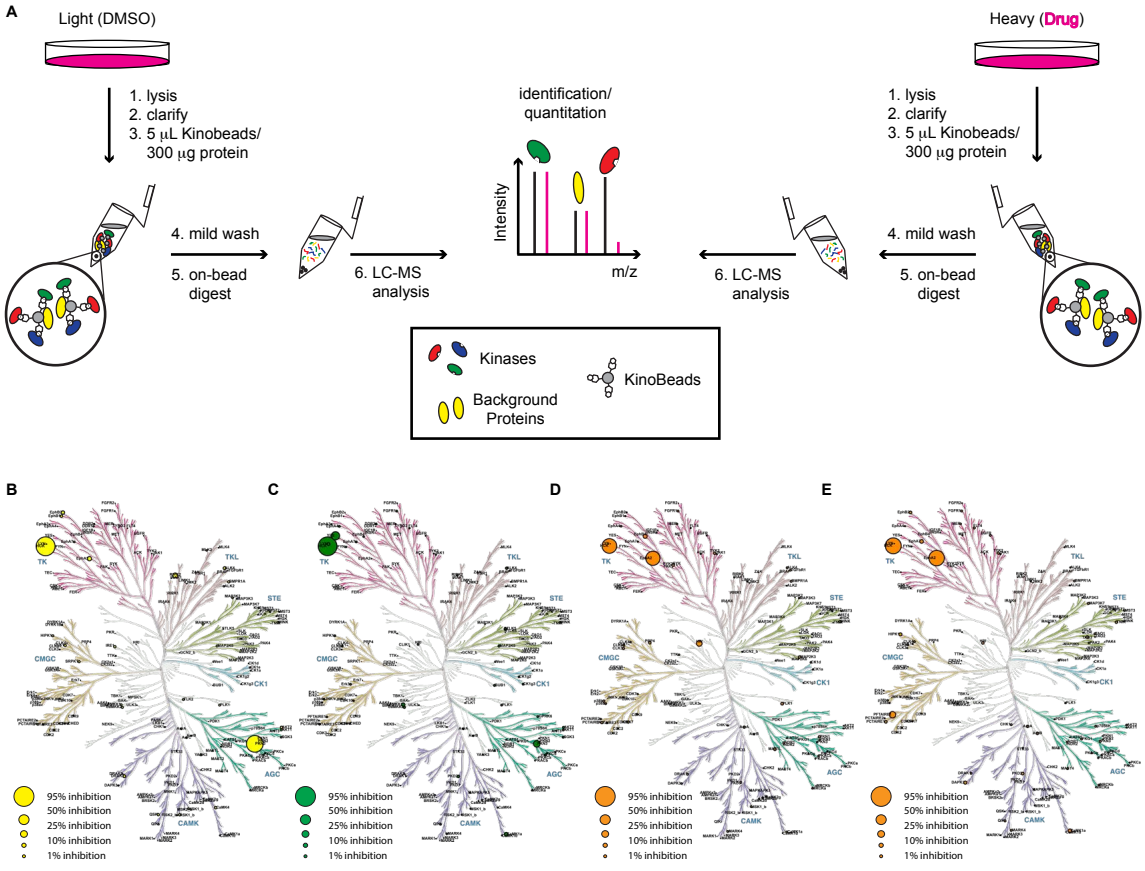

Figure 2- 3: Profiling against endogenous kinases in cell lysate demonstrates selectivity of 1-4

A. Experimental scheme describing the SILAC profiling experiment using KinoBeads. Kinases competed by free inhibitor (**1**, **2**, **3**, or **4**) are quantified at higher levels in the DMSO channel than the drug-treated channel (as seen with the red kinase in the theoretical spectrum). Kinases that are not inhibited show up as relatively equal in each channel. **B**. Results of profiling of ligand **1** mapped onto a kinase dendrogram. All profiled kinases are represented by circles and labeled by name. The size of the circle corresponds to relative percent competition (larger circle, more competed). **C**. Results for ligand **2** as described in B. **D**. Results for ligand **3** as described in B. **E**. Results for ligand **4** as described in B. Each profiling experiment was performed in triplicate.

The profiling results showed that the kinase PNK3 was depleted after treatment with all four inhibitors, most strongly with inhibitor **1**. An activity assay was preformed to test the affinity of the inhibitors for PKN3. Unfortunately, PKN3 is inhibited strongly by all four inhibitors. Since there is no available crystal structure of PKN3, it is hard to determine the mechanism of inhibition especially because there does not appear to be an active site Cys. As expected, RSK2 was also potently inhibited by the inhibitor panel in an activity assay; however, it did not appear to be depleted in the SILAC because RSK2 contains two kinase domains, only one of which is sensitive to the inhibitors. This is not surprising based on the results of the Taunton lab and the fact that RSK2 has an active site Cys. Since only one of the kinase domains of RSK2 contains an active site Cys and therefore is able to bind to inhibitors **1-4**, the other is able to bind to the KinoBeads and therefore is not competed away. Another off target kinase that was discovered in this screen was EPHA2, however after testing this kinase in an activity assay it appears that this kinase binds to inhibitors **3** and **4** at concentrations that are not physiologically relevant (**Figure2-2D**). EPHA2 was observed as being depleted in the screen because of the high concentration (50μM) of inhibitors used, however inhibition of EPHA2 can be avoided by using lower concentrations of the molecules. In this SILAC screen, only three off target endogenous kinases were observed to potently bind to our inhibitors. This proves that conformationally selective inhibitors **1-4** are highly selective for the analog sensitive kinase variants over endogenous kinases.

Table 2-1

Inhibitor	K_i RSK2 CTD	K_i PKN3
1	7 ± 2	10 ± 2
2	20 ± 3	110 ± 50
3	820 ± 180	520 ± 110
4	170 ± 30	26 ± 13

Table 2- 1: K_i values for 1-4 against RSK2 CTD and PKN3
All K_i values (nM) reported as mean ± SEM, n=3.

B. Biochemical characterization of kinases bound to conformation-selective inhibitors

After potent inhibition of the analog sensitive variants was observed in the SILAC experiment, the conformation of the kinases when bound to inhibitors **1-4** needed to be verified. Our lab has previously seen that stabilizing a kinase in a DFG-in or DFG-out and αC-helix out conformation causes the SH3 domain to have distinct accessibility. We have observed that stabilizing and ATP-binding site with DFG-in or DFG-out inhibitors causes the SH3 domain to be accessible to intermolecular binding partners (Leonard et al., 2014). When the kinase is in the active (DFG-in) conformation, it is in an open conformation and is free to engage with intermolecular binding partners and is highly susceptible to phosphorylation and dephosphorylation. When the kinase is in the inactive DFG-out conformation, the kinase remains in a state that is essentially the same as the active form of the kinase. The DFG motif moves 180° into a catalytically inactive state, but the αC-helix remains in the in conformation. However, when the αC-helix moves into the out position the kinase becomes autoinhibited and the SH2 and SH3 domains are

engaged. While in the αC-helix out conformation, the SH3 domain is engaged with it's intramolecular binding partner, the poly-Pro linker, and therefore is unavailable to bind with intermolecular binding partners. This occurs through *bi-directional*, allosteric communication between the αC helix and SH2-catalytic domain linker (Superti-Furga et al, 2000; Register et al, 2014)

Previously in our lab, we have been able to assess the accessibility of the SH3 domain using a pull-down assay (Leonard et al., 2014). In this assay, a peptide binding partner of the SH3 domain is conjugated to agarose beads. The degree of binding to the peptide conjugated to beads provides a means of assessing the accessibility of the SH3 domain. If the kinase is stabilized in the DFG-in or DFG-out conformations, the accessibility of the SH3 domain is increased and the SH3 domain of the kinase is retained on the beads. However, in the αC-helix out conformation, the accessibility of the SH3 domain is decreased and less kinase is retained on the SH3 binding resin (**Figure 2-4A**) (Leonard et al., 2014).

This pull-down experiment was preformed on Hck3D^{AS}, which was recombinantly expressed and purified from E. Coli (Seeliger et al., 2005). After incubation with inhibitors **1** and **3**, more Hck^{AS} was retained on the SH3 binding resin than after incubation with **2** (**Figure 2-4B)**. This experiment was repeated with recombinantly expressed and purified Abl3D^{AS}. The SH3 domain regulates Abl in a similarly to the SFKs: binding of the SH3 domain to the poly-Pro linker causing the αC-helix to rotate out, which causes auto-inhibition of the catalytic domain. Significantly higher amounts of Abl3D^{AS} bound to the SH3 after incubation

with **1** and **3** compared to incubation with **2** (**Figure 2-4C**). This result confirms previous NMR results that stabilizing a DGF-out conformation increases the SH3 domain accessibility of Abl. This result also suggests that the accessibility of the SH3 domain is regulated by the αC-helix, although Abl and SFKs have differences in structural regulation.

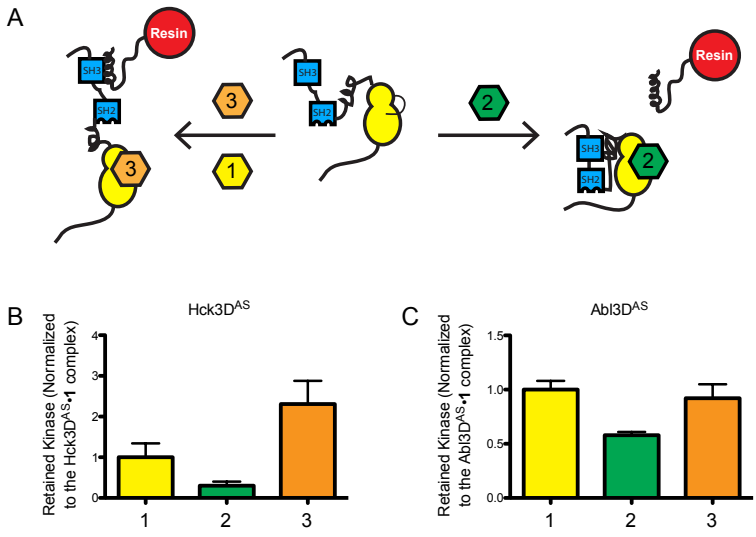

Figure 2- 4: 1-3 modulate Hck3D and Abl3D SH3 domain engagement by stabilizing their predicted ATP-binding site conformations

A. Experimental scheme for *in vitro* SH3 pull-down experiment. Type I- and DFG-out-stabilizing inhibitors (like inhibitors **1** and **3**) increase SH3 domain accessibility to an SH3 domain-binding peptide (left) compared to αC helix-out-stabilizing inhibitors (like inhibitor **2**), which decrease SH3 domain accessibility (right). **B**. Experimental results for Hck3D^{AS} retained on resin when bound to **1**, **2**, and **3**. All values are normalized to the Hck3D^{AS}•**1** complex and displayed as mean ± SEM, n=3. **C**. Experimental results for Abl3D^{AS} retained on resin when bound to **1**, **2**, and **3**. All values are normalized to the Abl3D^{AS}•**1** complex and displayed as mean ± SEM, n=3.

In order to verify that the kinases were in the expected conformations, Xray crystallography was preformed on Src^{AS} in complex with **1**, **2** and **3**. Gratifyingly,

the kinase conformation matched the expected results. In all three structures, the covalent bond between the kinase and the electrophilic inhibitor was observed. As expected, inhibitor **1** binds to Src in the active (DFG-in, αC-helix in) conformation (**Figure 2-5B-C**). Inhibitor **2** binds to Src in the αC-helix out inactive conformation, in which the αC-helix is rotated out of the active site, which displaces a catalytically important Glu. Our lab has previously found that the αC helix acts as a switch regulating both global kinase conformation and ability to undergo post-translational modification(**Figure2-5D-F**) (Leonard et. al. 2014). Inhibitor **3** binds to Src in the DFG-out, αC-helix in conformation (**Figure2-5G-I)**. Both **1** and **3** make a hydrogen bond with Glu310 in the αC-helix that is only possible when this structural motif is in an active conformation.

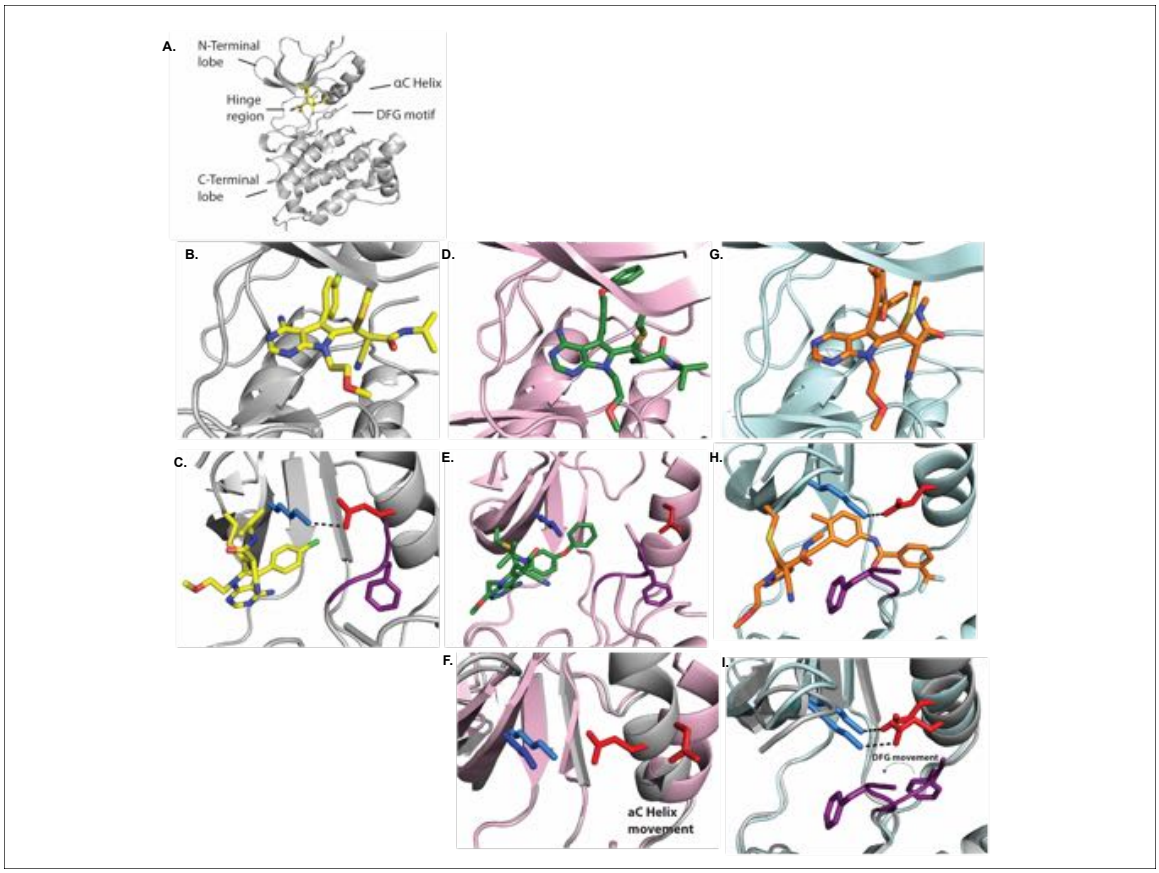

Figure 2-5: X ray crystallography confirms expected conformation of Src bound to inhibitors.

A. Structure of the kinase with **B.** As expected, inhibitor **1** (yellow) binds to Src in the active conformation. The pyrolpyrimidine scaffold binds in the ATP binding pocket and makes a hydrogen bond with the hinge region. **C.** The covalent linkage is observed between the inhibitor and Src Val281Cys. In this crystal structure, the kinase is an a DFG-in and αC-helix in conformation, where the salt bridge between Glu310 and Lys295 is maintained and stabilized by a hydrogen bond between the inhibitor and Glu310 (residues shown in blue). **D.** Inhibitor **2** (green) is covalently bound to Src Val281Cys and projects towards the αC-helix. **E.** The αC-helix is rotated out when inhibitor **2** is bound. **F.** The salt bridge between Glu310 and Lys295 is broken. **G**. Comparison of relative positions of the αC-helix. The αC-helix is rotated out when bound to inhibitor **2** compared to **1**. **H.** Inhibitor **3** (shown in orange) is covalently bound to Src Val281Cys. **I.** Inhibitor **3** projects towards the DFG motif, forcing it to rotate 180° into the DFG-out conformation (shown in purple) and is in the αC-helix in conformation, with the salt bridge maintained between Glu310 and Lys295 (shown in blue, inhibitor not shown). **J.** Comparison of the DFG motif after binding to **1** and **3.** When inhibitor **3** is bound, the DFG motif is flipped 180° relative to when inhibitor **1** is bound.

Pulldowns were also preformed in HEK293T cells over expressing Src^{AS} and Hck^{AS}, both labeled with a C-terminal Flag-tag. In this experiment, cells expressing Src^{AS} or Hck^{AS} were treated with inhibitors **1**-**3** for 2 hours, lysed and exposed to displaying the SH3 binding resin (**Figure 2-6)**. The amount of kinase retained on the beads was determined by probing for the Flag-tag on a Western blot. As expected, the same trend that was observed for the recombinant kinases was true, and more striking, for cellular kinases. As previously observed, the inhibitor dependent movement of the αC-helix is less coupled to the linker in Src than it is in Hck (**Figure 2-6 B-C)** (Register et al., 2014)., which accounts for the lower amount of retained kinase for Src. The accessibility of the SH3 domain was also greater after treatment with **3** than with **1**. This is possibly a result of the DFG-out ligand hydrogen bonding with Glu310 on the αC-helix, this could further stabilize the αC-helix in conformation compared to DFG-in ligands which do not have this hydrogen bond (Leonard et al., 2014). As expected, there was no difference in retained kinase for Hck^{WT} after treatment with **1**, **2** or **3** (**Figure 2-6 D**).

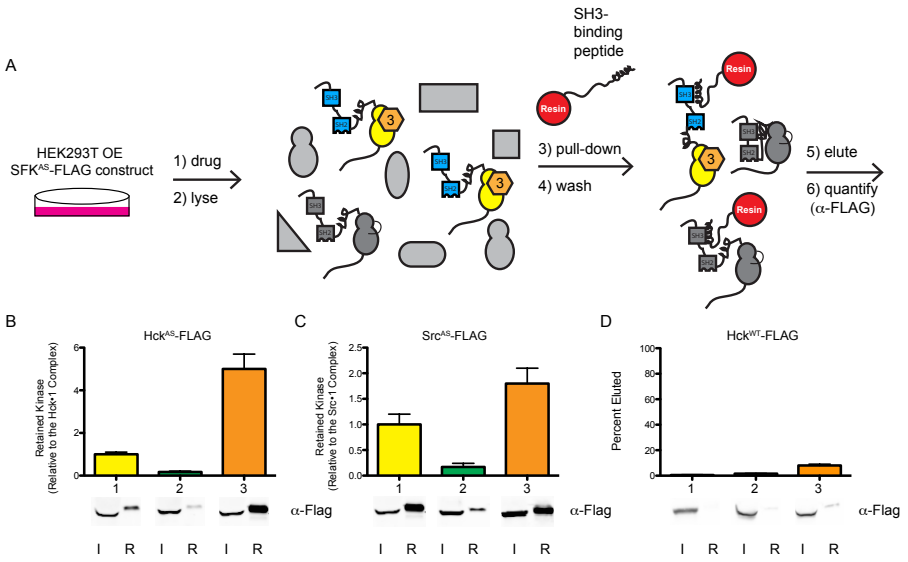

Figure 2-6: 1-3 modulate full-length SFK SH3 domain engagement in cells

A. Experimental scheme for cellular SH3 pull-down experiment. HEK293T cells overexpressing (OE) Flag-tagged full-length SFK^{AS} construct are treated with **1**, **2**, or **3** for 2 hrs before lysis, pull-down with SH3 domain-binding peptide resin, and quantitation of retained $kinase^{AS}$ via anti-Flag western blot. **B**. Quantification of retained Hck^{AS} bound to **1**, **2**, and **3** represented as bar graphs with representative anti-Flag blots (I: input kinase; R: retained kinase). All data is normalized to the Hck^{AS}•**1** complex and displayed as mean ± SEM, n=3. **C**. Quantification of retained Src^{AS} bound to **1**, **2**, and **3** represented as bar graphs with representative anti-Flag blots (I: input kinase; R: retained kinase). All data is normalized to the Src^{AS}•**1** complex and displayed as mean ± SEM, n=3 **D**. Quantification of retained Hck^{WT} when incubated with **1**, **2**, or **3** represented as bar graphs. Data is represented as Percent Retained HckWT and displayed as mean ± SEM, n=3.

In order to further validate the conformationally selective inhibitors and learn more about the impact they have on biologically relevant phosphorylation events, an experiment was designed to measure C-terminal tail phosphorylation of Src by Csk. Csk is a suppressor of Src family kinase activity, by phosphorylating a conserved tyrosine residue on the C-terminal tail of the SFK. This phosphorylation results in an increased affinity of the C-terminal tail for the SH2 domain thereby inactivating the kinase. (Okada et al., 1991; Levinson et al., 2008). In this assay, Src is stabilized in an inhibitor dependent DFG-in, DFG-out or αC-helix out

conformation, resulting in differential accessibility and phosphorylation of the C-terminal tail. As seen previously, stabilizing the kinase in a DFG-in or DFG-out conformation with **1** and **3** respectively should increase the accessibility of the regulatory domains and the C-terminal tail and result in high phosphorylation by Csk. Conversely, the αC-helix out conformation should decrease the accessibility of the regulatory domains and the C-terminal tail and result in less phosphorylation by Csk (**Figure 2-7A)**. In this experiment, Src^{AS} was incubated with inhibitors **2** and **3** at a level at which all of the Src was bound to the inhibitor, but such that Csk was uninhibited. High structural homology typically results in inhibitors that inhibit both SFKs and Csk, however the analog sensitive Src overcomes this issue and allows an inhibitor of Src to be used in the presence of Csk with no inhibition observed. In this experiment, only inhibitors **2** and **3** were used because they showed the greatest difference in effect based on the previous experiment. An activity assay was preformed to determine the level of C-terminal Tyr527 tail phosphorylation by measuring the level of γP^{32} retained on nitrocellulose. The results were as expected: after treatment with **3** Src^{AS} and Hck^{AS} showed a respective 3-fold and 9-fold increase in phosphorylation compared to treatment with **2** (**Figure 2-7B**). As seen in the previous experiment, the movement of the αC-helix is allosterically coupled to accessibility of the SH3 domain to a higher degree in Hck than it is in Src. This is supported by previous SH3 pulldowns reported by our lab (Register et. Al. 2014.)

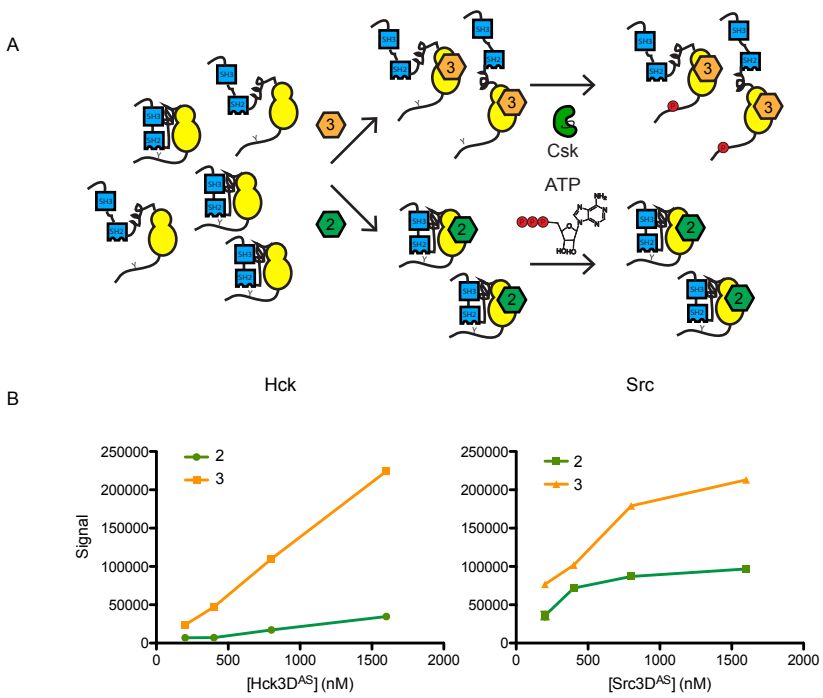

Figure 2-7: Stabilization of DFG-out and αC helix-out ATP-binding site conformations with 3 and 2 divergently modulates SFK pTyr527 by Csk

A. Experimental scheme for SFK Y527 phosphorylation assay. SFK3D^{AS} was incubated with **2** or **3** for 1 hr before addition of Csk and γP^{32}-ATP. Accessibility of Tyr527 for phosphorylation by Csk is modulated by inhibitor-driven conformational changes. **B.** Results for Hck3D^{AS} and Src3D^{AS} bound to **2** (green) and **3** (orange) reported as mean ± SEM, n=3.

In order to verify that the differences observed in the previous experiment are driven by the conformation of the kinase and not catalytic activity of the kinase, an experiment was preformed with a kinase dead mutant of the kinases that was not sensitized to the inhibitors. The K295M kinase dead mutation (SFK3D^{KM}) insures that autophosphorylation of the SFK will not obscure the phosphorylation of Tyr527. As expected, there was no difference in tail phosphorylation after incubation with DMSO, **2** or **3** for either Src3D^{KM} or Hck3D^{KM} (**Figure 2-8B).** This was anticipated because **2** and **3** have little affinity for the binding site of the analog insensitive mutants. To further confirm

that the differential C-terminal phosphorylation of Csk is a result of differential SH2 domain accessibility, an experiment was preformed with Src and Hck that consisted of only the catalytic domain and the C-terminal tail ($SFKCD^{AS}$; **Figure 2-8C**). In this experiment, there was no difference in phosphorylation between $SrcCD^{AS}$ and $HckCD^{AS}$, which supports our hypothesis that the active site conformation of the kinase is allosterically driving accessibility of the SH2 domain. These results confirm that both the analog sensitizing mutation and the regulatory domains are required for the observed differences in C-terminal tail phosphorylation by Csk. In summary, these results show that stabilizing the kinase in an DFG-in, DFG-out or αC-helix out conformation have differential effects on the phosphorylation state of the kinase. In order to probe the biological impacts of these divergent effects, cellular experiments were preformed to connect ATP binding site conformation to phenotype of the cell.

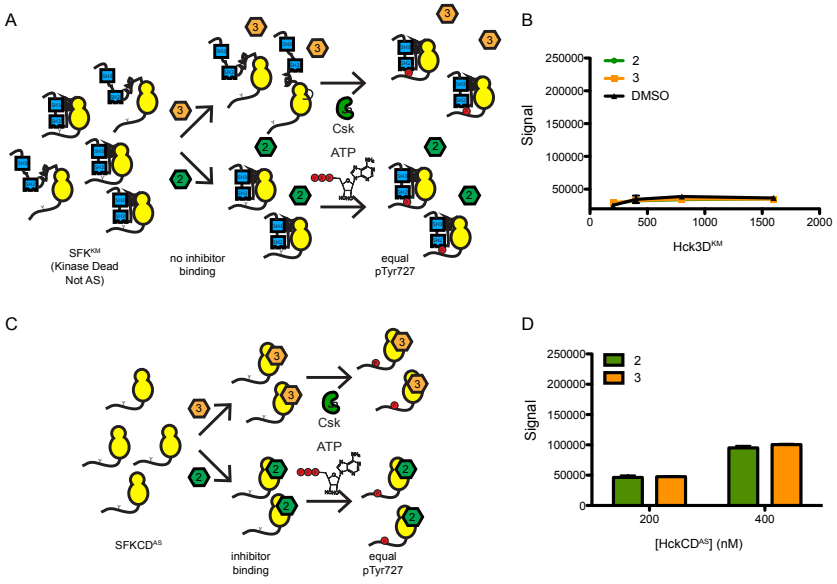

Figure 2-8: Inhibitor-binding effects on pTyr527 require AS mutation and regulatory domains

A. Experimental scheme for SFK Tyr527 phosphorylation assay using a kinase dead, analogue-insensitive SFK construct. Hck3D^{KM} was incubated with **2** or **3** for 1 hr before addition of Csk and γP^{32}-ATP. Accessibility of Tyr527 for phosphorylation by Csk is not modulated by inhibitor-driven conformational changes because inhibitors do not bind to the active site of Hck3D^{KM}. **B**. Results for Hck3D^{KM} incubated with **2** (green), **3** (orange), and DMSO (black) reported as mean ± SEM, n=3. **C**. Experimental scheme for SFK Tyr527 phosphorylation assay using an SFKCD^{AS} construct. SFKCD^{AS} was incubated with **2** or **3** for 1 hr before addition of Csk and γP^{32}-ATP. Accessibility of Tyr527 for phosphorylation by Csk is not modulated by inhibitor-driven conformational changes because SFKCD^{AS} lacks SH3 and SH2 regulatory domains. **D**. Results for HckCD^{AS} bound to **2** (green) and **3** (orange) reported as mean ± SEM, n=3.

C. Stabilizing the Src^{AS} ATP-binding site in a DFG-out conformation increases Src co-localization with the plasma membrane, blebbing, and motility in fibroblasts

To assess ATP-binding site conformation dependent effects on Src localization, fixed-cell confocal microscopy was performed on Src/Yes/Fyn (-/-) 3T3 cells (SYFs) transiently transfected with Src^{AS}-GFP (C-terminal GFP construct). The localization of Src^{AS} at the PM, cytosol, Golgi apparatus and endosomal membranes matched previously published results (Resh et al, 2008) and is similar to Src^{WT}-GFP. Transfected cells were treated with 3 μM **2** or 1μM **3** for 15 min, before fixation and staining with a wheat germ agglutinin AlexaFluor 647-conjugate, for visualization of the plasma membrane and DAPI. Incubation with 1mM **3** resulted in a depletion of Src^{AS}-GFP in the cytosol and enchancement of Src^{AS}-GFP localization at the plasma membrane and Golgi bodies that was not observed when Src^{AS}-GFP was treated with 3μM **2** or DMSO (**Figure 2-9A**). Treatment with **1** showed localization that was less dramatic than localization after treatment with **3** (**Figure 2-10B)**. Performing the identical experiment on SYF cells over expressing Src^{WT} showed no apparent difference in Src localization between treatments with **3** and DMSO, indicating that the inhibitors are acting exclusively

on the analog sensitized mutant (**Figure 2-10A**). In order to rule out the possibility that the differential effect of **2** and **3** is due to engagement with Src on differing time scales, a competition experiment was preformed by co-administering 1mM **3** and 3mM **2** (**Figure 2-9A,C**)**.** Simultaneous treatment with the inhibitors for 15 minutes showed localization similar to treatment with **2** alone, proving that compound **2** is cell permeable and functions on the same time scale as compound **3**. It was observed that a higher concentration of **3** gave more robust localization, so 10μM **3** was used for all subsequent experiments.

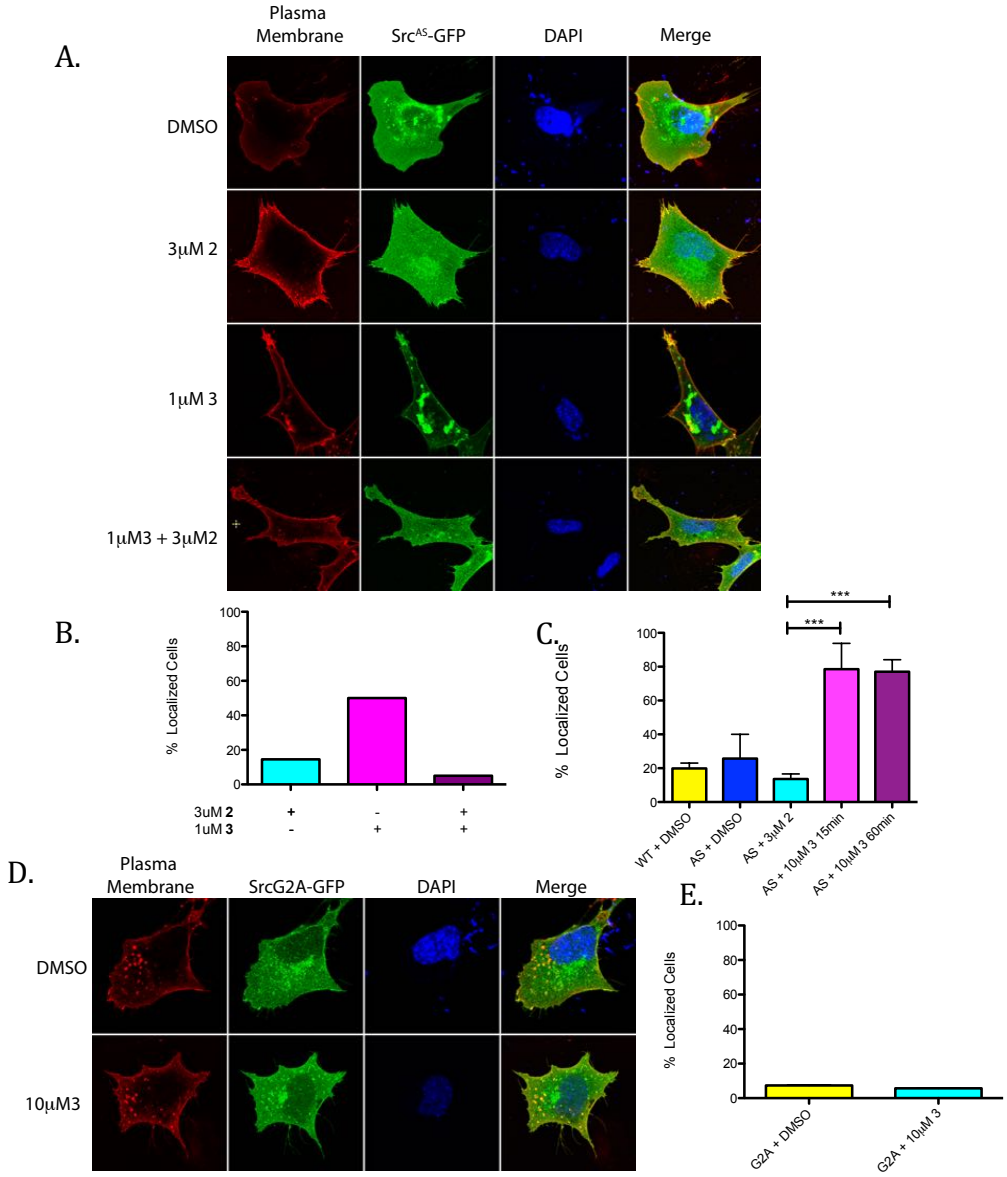

Figure 2-9: SrcAS localizes at plasma membrane by stabilizing SrcAS in a DFG-out conformation.

(A) SYFs expressing SrcAS-GFP were treated with the indicated inhibitors in a competition experiment for 15 minutes, fixed and stained for the PM and nucleus. Shown are representative confocal micrographs. (B) Quantitative analysis of localization in competition experiment. n=1, 15 cells per condition. (C) Quantitative analysis of localization following inhibitor treatment. SYFs were treated with the indicated drugs for 15 minutes, fixed stained for the PM and evaluated for PM localization by three unbiased scorers. Values are the arithmetic means of 3-7 experiments +s.d. In each experiment, 8-30 cells were counted per condition. (D) Unmyristoylated Src does not localize at the plasma membrane. SYFs expressing SrcG2A, a mutant with the myristoyl acceptor glycine at position 2 replaced by alanine. Cells were treated with the indicated inhibitor

fixed and stained for the PM and nucleus. Shown are representative confocal micrographs. (E) Quantitative analysis of localization following inhibitor treatment. SYFs were treated with the indicated drugs for 15 minutes, fixed stained for the PM and evaluated for PM localization. Values are the arithmetic means of 2 experiments +s.d. In each experiment, over 15 cells were counted per condition.

The N-terminus of Src contains an SH4 domain, which consists of a myristoylated glycine followed by four basic amino acids. The SH4 domain is required to target Src to the plasma membrane, which has important implications for cell migration (David-Pfeuty et al., 1993). Introducing a G2A mutation in the SH4 domain of Src^{AS}-GFP —to prevent myristoylation of the N-terminus— resulted in localization of Src^{G2A}-GFP in the cytosol after treatment with DMSO (**Figure 2-9D,E**). Treatment with 10μM **3**, resulted in Src^{G2A}-GFP a similar distribution to DMSO treatment, with no enhanced co-localization at the plasma membrane or depletion of cytosolic Src^{AS}-GFP(**Figure 2-9D,E**). N-terminal myrsitoylation is necessary for enhancement of Src^{AS}-GFP at the plasma membrane after treatment with **3**. It appears that N-terminal localization is connected to the accessibility of the SH2 and SH3 domains.

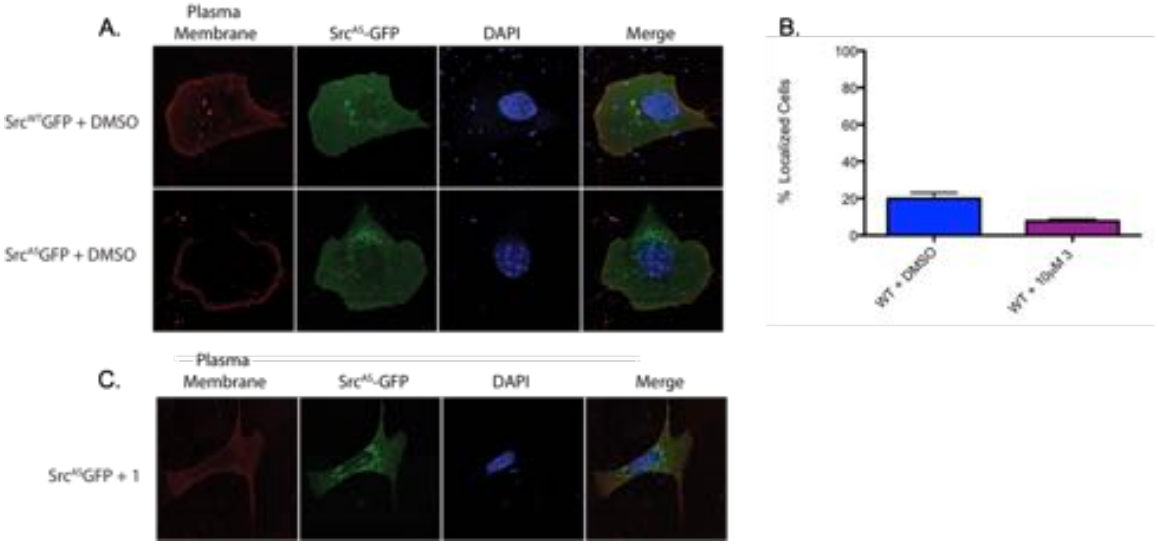

Figure 2-10: Localization of Src^{WT}-GFP compared to Src^{AS}-GFP

(A) Src^{AS}-GFP localization is similar to Src^{WT}-GFP. SYFs expressing Src^{WT}-GFP or Src^{AS}-GFP were treated with DMSO for 15 minutes, fixed and stained for the PM and nucleus. Shown are representative confocal micrographs. (B) Quantitative analysis of localization following DMSO or inhibitor treatment. SYFs were treated with the indicated drugs for 15 minutes, fixed stained for the PM and evaluated for PM localization by three unbiased scorers. Values are the arithmetic means of 2 experiments +s.d. In each experiment, 15-30 cells were counted per condition. (C) Src^{AS}-GFP treated with **1** shows localization that is less dramatic than treatment with **3**. SYFs expressing Src^{AS}-GFP were treated with **1** for 15 minutes, fixed and stained for the PM and nucleus. Shown are representative confocal micrographs.

Interestingly, while performing these experiments, we also noticed an increase in membrane blebs—dynamic cytoskeleton-regulated membrane protrusions important for cell motility and invasiveness—when SYF cells reconstituted with Src^{AS}-GFP were treated with 10mM **3** (**Figure 2-11A,B,D**). Markedly fewer membrane blebs were observed for SYF cells reconstituted with Src^{AS}-GFP after treatment with DMSO or **2** (**Figure 2-11B)**. Similarly, SYFs reconstituted with Src^{WT} treated with either DMSO or **3** (Fackler and Grosse, 2008) showed few membrane blebs, indicating that the inhibitor is acting on target and that blebbing is not a function of the inhibitor alone (**Figure 2-12)**. A competition was preformed with coadministration of 10mM **3** and 3mM **2** (**Figure 2-11C**)**.** PM blebbing was observed to be comparable to addition of **2** alone proving that both inhibitors are working on a similar time scale.

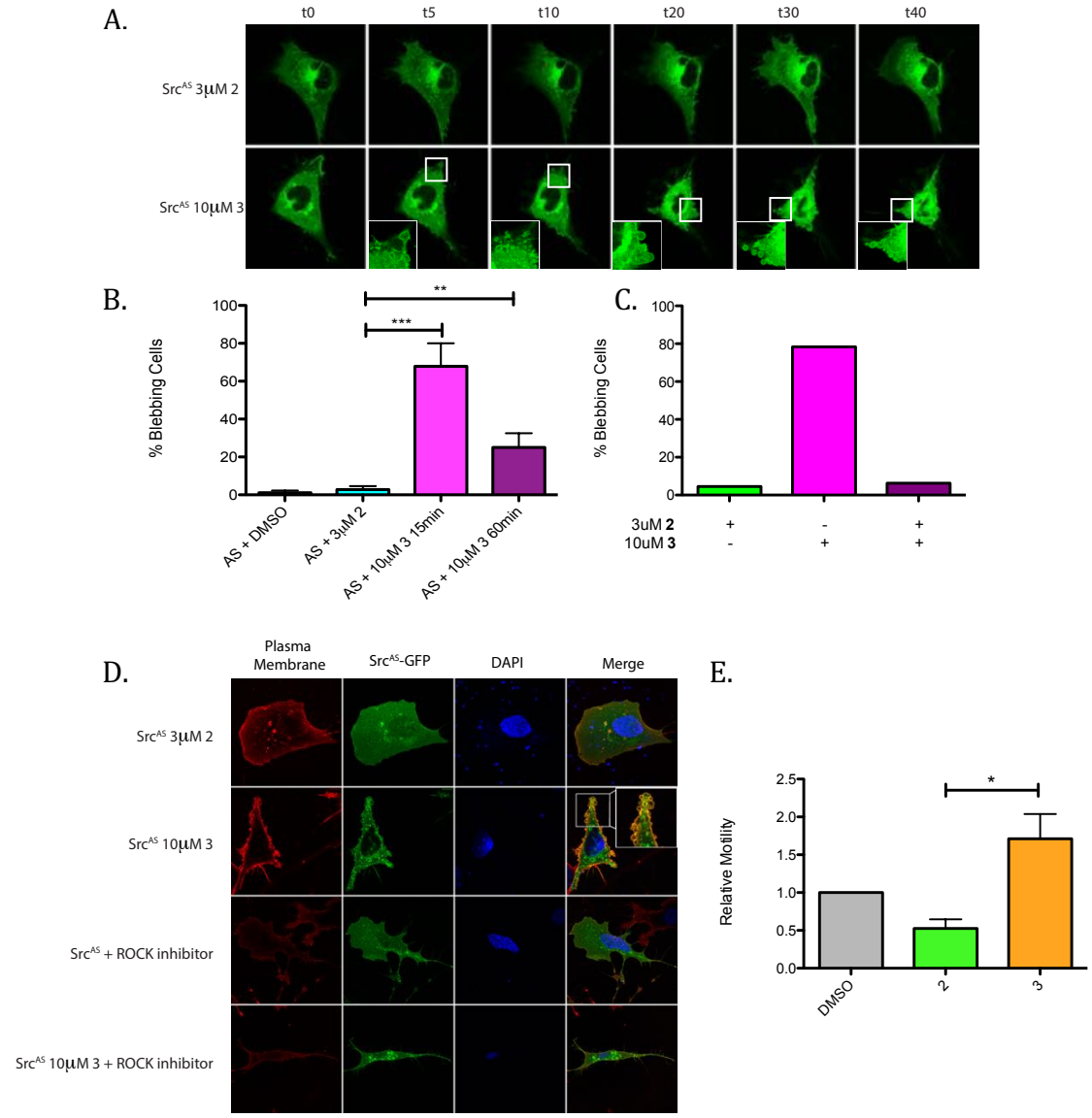

Figure 2-11 Blebbing is initiated by stabilizing SrcAS in a DFG-out conformation.

(A) Still frames captured from time-lapse confocoal microscopy of live SYFs expressing SrcAS-GFP. Arrows indicate blebs forming at the PM. (B) Quantitative analysis of blebbing following inhibitor treatment. SYFs were treated with the indicated inhibitors for 15 minutes, fixed stained for the PM and evaluated for PM localization by three unbiased scorers. Values are the arithmetic means of at least 3 experiments +s.d. In each experiment, over X cells were counted per condition. (C) Blebbing is reversible and therefore a non-apoptotic result of stabilizing the DFG-out conformation. Quantitative analysis of blebbing following competition experiment. SYFs were treated with the indicated inhibitors for 15 minutes, fixed stained for the PM and evaluated for PM localization by three unbiased scorers. (D) SYFs expressing SrcAS-GFP were treated with

the indicated inhibitors experiment for 15 minutes, fixed and stained for the PM and nucleus. Cells were treated with Gsk429286a, a ROCK inhibitor, for 2 hours prior to a 15 minute treatment with 3. Localization of SrcAS at the plasma membrane is not su cient to cause PM blebbing, active ROCK is required. (E) Blebbing caused by stabilizing SrcAS in the DFG-out conformation correleates with enhanced cell migration in 3D matricies. SYF cells expressing SrcAS were treated with the indicated inhibitor for 24 hours and migration across matrigel coated transwells was assessed. Values are the artithmetic means of three independent experiments. Statistical significance was evaluated using the student's T test.

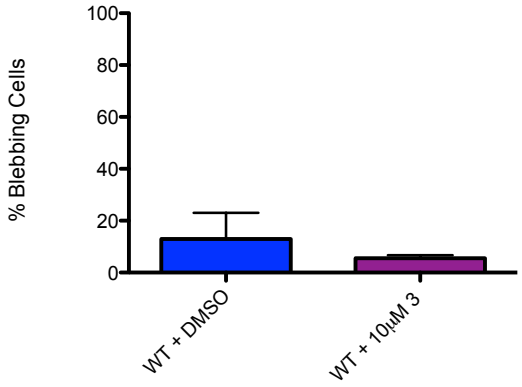

Figure 2-12: Membrane blebbing of WT Cells after inhibitor treatment
(A) Quantitative analysis of blebbing in Src^{WT}-GFP following DMSO or treatment with **3**. SYFs were treated with the DMSO or indicated inhibitor for 15 minutes, fixed stained for the PM and evaluated for PM blebbing by three unbiased scorers. Values are the arithmetic means of 2 experiments +s.d. In each experiment, 15-30 cells were counted per condition.

In order to observe the impact of inhibitors **2** and **3** on PM blebbing with other SFKs, SYFs co-expressing non-GFP tagged Fyn^{AS} and GFP were treated with 10mM **3** or 3mM **2** (**Figure 2-13A,B**)**.** Like Src^{AS}-GFP treated with **2**, Fyn^{AS} showed low blebbing. Treatment with **3** showed an increase in PM blebbing. Treatment with **3** caused the same phenotype in both Src and Fyn despite the fact that the SH4 domain of Fyn is both palmityolated and myristoylated confirming that the type of acylation does not have an impact on PM blebbing.

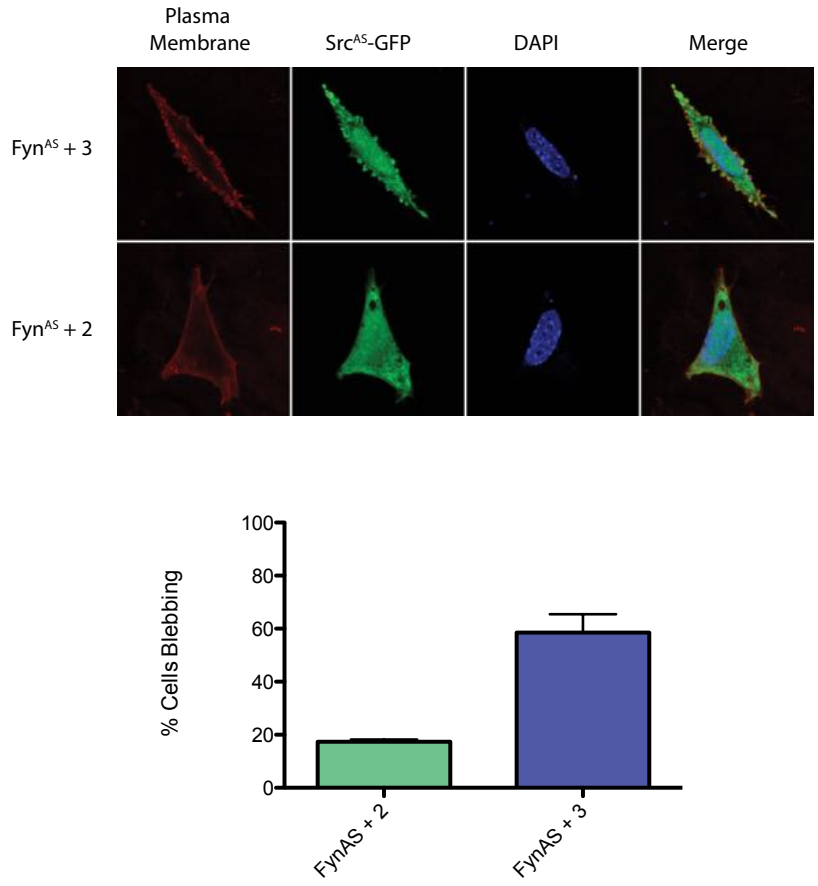

Figure 2-13: Membrane Blebbing of Fyn
(A) Blebbing is initiated by stabilizing Fyn^{AS} in a DFG-out conformation. SYFs co-expressing Fyn^{AS} and GFP were treated with the indicated inhibitors for 15 minutes, fixed and stained for the PM and nucleus. Shown are representative confocal micrographs. (B) Quantitative analysis of localization following inhibitor treatment. SYFs co-expressing Fyn^{AS} and GFP were treated with the indicated drugs for 15 minutes, fixed stained for the PM and evaluated for PM blebbing by two unbiased scorers. Values are the arithmetic means of 3 experiments +s.d. In each experiment, 15-20 cells were counted per condition.

To further determine the impact of inhibitors **2** and **3** on membrane bleb formation, we next preformed a confocal real-time imaging analysis on SYFs reconstituted with Src^{AS}-GFP (**Figure 2-11A and supplementary material Movies 1-3).** To gain further insight into this dynamic process, we initially looked at a 15-minute treatment with 3μM **2** and found no change in localization or blebbing. Monitoring over 60-minutes confirmed the result. In contrast, treatment with 10μM **3** caused blebbing initiation at 5 minutes (**Figure 2-11D)**. Further

monitoring over a 40-minute period showed continued formation of PM blebs, consistent with non-apoptotic blebbing induced by SH4 domains as previously reported (Tournaviti et al., 2007) (supplemental movies 1-4). Association of Src's N-terminal SH4 domain with the plasma membrane has previously been shown to be associated with an increase in blebbing, providing further evidence that stabilizing the ATP-binding site of Src in a DFG-out conformation with ligand **3** is increasing Src's localization with the plasma membrane, presumably by allosterically increasing SH3 and SH2 regulatory domain accessibility and exposing the SH4 domain. (Tournaviti et al., 2007).

The Rho effector kinase Rock has been shown to be involved in PM blebbing by providing acto-myosin contractibility. Inhibition of Rock has been shown to abolish PM blebbing induced by SH4 domains (Tournaviti et al. 2007). Treating SYFs expressing Src^{AS} with Rock inhibitor Gsk429286a and **3** simultaneously, resulted in localization of Src^{AS}-GFP **3** at the plasma membrane, but caused a potent interference of PM blebbing (**Figure 2-11D**). This result confirms that Rock is downstream of SH4 localization and is necessary and for SH4 induced plasma membrane blebbing. It also indicates that the observed blebbing is dependent on acto-myosin contractibility. The behavior of Src^{AS}-GFP after treatment with **3** mimics the behavior of the SH4 domain of Src alone as previously reported by (Tournaviti et al, 2007). This suggests that the SH4 domain is shielded in the αC-helix out conformation of full length Src, but in the DFG-out conformation caused by treatment with **3**, the SH4 domain is exposed.

Given the observation that the SH4 domain of Src, but not Src catalytic activity, is necessary to restore cell motility in fibroblasts, we were curious whether treatment with our conformation-selective inhibitors would modulate Src's ability to enhance cell motility. A standard transwell motility assay was performed on SYFs reconstituted with or Src^{AS}-GFP, wherein the migration of cells through a membrane is quantified. The data is normalized to cells treated with DMSO. Cells treated with 10μM **3** exhibited 4-fold more movement through the matrix compared to cells treated with 3 μM **2**, indicating that the short-term blebbing previously observed translates into cell migration over a longer time period. This result suggests that stabilizing a DFG-out ATP-binding site conformation increases Src's ability to enhance motility in fibroblasts, presumably a result of blebbing associated cell motility. (**Figure 2-11E**). This result provides further evidence that Src's important role in cell motility is played largely through by increasing accessibility of the SH3 and SH2 regulatory domains, which leads to exposure of the SH4 domain.

III. Conclusion

In this work we have presented a novel chemical-genetic strategy that can be was used to investigate the impact of ATP-binding site conformation on a kinase of interest. In order to study the impact of ATP-binding site conformation on kinase non-catalytic activity, a panel of covalent inhibitors (**1**-**4**) were generated and shown to stabilize either Type I/active, αC helix-out, or DFG-out ATP-binding site conformations thorough biochemical characterization of their allosteric effects on SFK regulatory domain engagement. Crystal structures of the inhibitors (**1**-**4**) bound to the kinase confirmed the expected conformation of the kinase. The

selectivity demonstrated in this system through making analog sensitive variants of Src, Hck, Abl, EphA2, and Pak1 that only show a few off target effects, prove that this methodology has the capacity to be expanded to any kinase to study non-catalytic function.

A tool set that allows for probing non-catalytic function of kinases will be useful for studying non-catalytic function of kinases. As we have shown, phosphorylation and localization are dramatically impacted by the conformational state of the kinase. We found that stabilizing a DFG-out conformation of the kinase increases membrane localization, blebbing and cell motility in fibroblasts presumably by allosterically increasing SH3 and SH2 regulatory domain accessibility and exposing the SH4 domain. Certainly, further research to separate the catalytic roles and non-catalytic roles of protein kinases is needed and can play a key role in drug development. For example, stabilizing Src in a DFG-out (catalytically inactive) conformation resulted in an increase in cell motility. This means that a drug that stabilizes the DFG-out ATP binding site conformation could cause an increase in cell motility, which is the opposite of the desired outcome.

Exciting advances in the field of gene editing can potentially allow the introduction of the analog sensitizing mutation to be expanded to virtually any endogenous kinase in any cell type in order to observe phenotypic differences. This would allow researchers to determine the impacts of ATP binding site conformation on cellular signaling and potentially avoid avoiding scenarios like the paradoxical activation of CRAF by Type I- and DFG-out-stabilized BRAF (Poulikakos et al., 2010; Hatzicassiliou et al., 2010; Zhang et al., 2015).

IV. Materials and Methods

A. Cloning and protein expression

Analogue-sensitizing mutations were engineered using site-directed mutagenesis. To pick mutation site, the catalytic domain sequences of Hck, Src, Abl, EphA2, Erk2, and PAK1 were aligned with the RSK2 CTD and Val residue corresponding to Cys436 in the RSK2 CTD (numbering varies for each kinase).

Src3D, Hck3D, and Abl3D constructs were expressed and purified as described previously (Seeliger et al., 2005; Register et al., 2014; Leonard et al., 2014). His-tagged Erk2, EphA2 catalytic domain, and Pak1 catalytic domain constructs were grown to OD 1.2 in 2 L flasks of LB in a shaking incubator at 37°C. The temperature was dropped to 18°C for 1 hr before induction with 0.2 mM IPTG. Overexpression proceeded overnight at 18°C before cells were harvested by centrifugation, lysed by sonication in lysis buffer (50mM HEPES, 150 mM NaCl, 20 mM Imidazol, 10 mM PMSF, 0.1% Triton-X 100 pH 8.0), and cleared for 40 min at 10000xg. Cleared lysates were incubated to 500 μL Ni-NTA resin for 1 hr, after which the lysate was discarded and beads were washed with 20 mL lysis buffer before bound protein was eluted with lysis buffer containing 300 mM imidazole. Eluted protein was analyzed for purity by SDS-PAGE and dialyzed overnight in 1 L dialysis buffer (50mM Tris, 150 mM NaCl, 1 mM DTT, 5% glycerol pH 8.0) at 4°C.

c-Abl1b was purchased from Addgene (plasmid #31284) and cloned into pcDNA5/FRT/TO (Invitrogen, product number V6520-20) using Gibson Assembly (NEB, product number E2611L). Overlap extension PCR was used to install GSGT-Flag sequence (GSGTDYKDDDDK) to the C-terminus of c-Abl immediately before the Stop codon to generate C-terminally Flag-tagged c-Abl constructs. Full-length Src and Hck were cloned into pcDNA5/FRT/TO and Flag-tagged using the same method. The Src C-terminal GFP fusion was generated by Gibson Assembly of PCR amplified Src (no tag) and GFP with PCR-linearized pcDNA5/FRT/TO.

B. Cell culture, stable cell line generation, and transient transfection conditions

Flp-In T-REx 293T (Invitrogen, product number R78007), SYF 3T3s, and HeLa cells were maintained in DMEM (Gibco, product number 11065092) supplemented with 10% FBS (Gibco, product numberA3160602). Dox-inducible stable 293Ts were generated using the Flp-In T-REx system as described in product documentation, and maintained with 50 μg/mL hygromycin and 15 μg/mL blasticidin after selection. All transient transfections were done using Turbofectin8.0 (OriGene) at a ratio of 3:1 μL Turbofectin: μg DNA (HeLa cells) or 4:1 (SYF cells) prepared in serum-free DMEM 12-24 hrs after plating of cells. Transfections were allowed to proceed 24-48 hrs before experiments were performed.

C. SILAC cell culture

Flp-In T-REx 293T cells were grown in custom -Lys/-Arg DMEM (Caisson Labs, North Logan, UT) supplemented with 10% dFBS (Sigma, St Louis, MO), 200 µg/ml proline and SILAC amino acids (0.2 mM Lys0/Arg0 for light label, 0.2 mM Lys8/Arg10 for heavy label; Cambridge Isotope Labs, Andover, MA). Cells were grown for at least 5 cell doublings in SILAC medium and harvested when reaching 90% confluency and after induction with 0.5 mg/mL doxycycline (dox.) to induce Hck^{AS} or c-Abl^{AS} overexpression (24 hr overexpression).

D. Activity assays to determine IC_{50}s for 1-4 against $Kinase^{AS}$ and $Kinase^{WT}$

All assays were performed in assay buffer (75 mM HEPES pH 7.5, 150 mM NaCl, 15 mM $MgCl_2$, 3.75 mM EGTA, 1 mM Na_2VO_3, and 1 mM DTT). Abl3D, Hck3D, and Src3D AS and WT constructs were assayed using a self-reporting, fluorometric assay utilizing Pyrene-Dap containing peptide substrates (Wang et al., 2006; Abl pyrene peptide sequence: Ac-AEAIYAA(dap-pyrene)-LA- NH2 and SFK pyrene peptide sequence: Ac-EEEITGE(dap-pyrene)-EA-NH_2). Titrations of inhibitors (3-fold serial dilutions starting at 30 µM, eight data points) were assayed in a black 384-well plate (Corning, product number 3573) in assay buffer containing 30 nM $Abl3D^{WT}$, 38 nM $Abl3D^{AS}$, 7.5 nM $Hck3D^{WT}$, 7.5 nM $Hck3D^{AS}$, 8 nM $Src3D^{AS}$, or 10 nM $Src3D^{WT}$ and 1 mM ATP the final volume per well for each assay was 30 µL and the final DMSO concentration was 4%. Enzymatic reaction was initiated with Abl/SFK pyrene substrate after 1-hr incubation at room temperature of Abl3D, inhibitor, and ATP. The reaction proceeded for 2 hrs after which the plate was read on a Perkin Elmer EnVision fluorimeter (Ex 340, Em 405). Data was exported to

excel, quantified as percent Abl inhibition, and plotted using Prism Graphpad software.

ppErk2^{AS} (1.5 nM), ppErk2WT (3 nM), EphA2^{WT} (2.5 nM), EphA2^{AS} (7 nM), Pak1^{WT} (x nM), and Pak1^{AS} (x nM) were assayed at a substrate-limiting ATP concentration using γ32-ATP (final concentration 0.0067 μCi per well). The Erk2^{AS} construct contained DFG-out-inhibitor sensitizing mutations (Hari et al., 2014), and the EphA2 and Pak1 constructs tested consisted only of the kinase catalytic domains. The final volume of each assay well was 30 µL. Myelin Basic Protein (MBP, final concentration 0.1 mg/mL) was used as a substrate for Erk2 and Pak1 assays, while 4:1 Glu:Tyr peptide substrate (Sigma, P0275; final concentration 0.1 mg/mL) was used for EphA2. The enzymatic reactions were initiated by the addition of γ32-ATP, run at room temperature for 2 hrs, and terminated by spotting 4.6 µL of the reaction mixture onto a phosphocellulose membrane. Membranes were washed with 0.5% phosphoric acid (3x, 10 minutes each wash), dried, and the radioactivity was determined by phosphorimaging with a GE Typhoon FLA 9000 phosphor scanner. The scanned membranes were quantified with ImageQuant. Data was analyzed using Prism Graphpad software.

E. Inhibitor selectivity profiling

Kinase affinity and sample enrichment: For kinase enrichment, 20 µl of a 50% kinobead slurry in 20% aqueous ethanol was pipetted into a 1.5 ml microtube and washed twice with 200 µl of mod. RIPA buffer (50 mM tris, 150 mM NaCl, 1% NP-

40, 0.25% Na-deoxycholate, 1 mM EDTA and 10 mM NaF, pH = 7.8 with 1x Halt™ Protease Inhibitor Cocktail (100x, Thermo Scientific, Rockford, IL)). In parallel 600 µg of cell extract in mod. RIPA buffer (ca. 4 mg/ml protein concentration) from either light or heavy labeled cells was pipetted into a 1.5 ml micro tube for each pulldown. The inhibitor in DMSO (competitor, 100x) or pure DMSO (control) was added to the corresponding SILAC lysate (1% DMSO final conc.) and the tubes were agitated for 20 min at 4°C on a rotator. For the SILAC label swap experiment the addition of competitor to e.g. the light lysate was switched to heavy lysate, and addition of the DMSO ctrl to the heavy lysate was switched to light lysate. After the 20 min incubation the pretreated lysate was pipetted individually to the tubes containing kinobead affinity resin and the slurry was agitated on a rotator for 3 hrs at 4°C. The supernatant was removed and the beads were washed twice with 200 µl of ice cold mod. RIPA buffer. Then the beads were re-suspended in 200 µl of ice cold TBS (50 mM Tris, 150 mM NaCl, pH = 7.8), the SILAC samples (beads) were combined pairwise (competition and ctrl experiments) and the supernatant was removed. The beads were washed twice more with TBS and then re-suspended in 100 µl of 8 M aq. urea containing 5 mM *tris*-(2-carboxyethyl)phosphine (TCEP) and 10 mM 2-chloroacetamide (CAM). The bead slurry was agitated for 30 min at 37°C and 1400 rpm on a thermomixer. For digestion, the slurry was diluted two-fold with 100 mM aqueous triethylammonium bicarbonate solution (TEAB, urea concentration ≤4 M), the pH was adjusted to 9 with 1 N NaOH and 1 µg of LysC was added. The slurry was shaken for 2 hrs at 1400 rpm and 37°C. Then the slurry was further diluted 2-fold with 100 mM TEAB

(urea concentration ≤2 M) and 1 µg of trypsin per 5 µl of affinity resin was added. Samples were digested overnight on a thermo shaker at 37°C, diluted two-fold with 5% aqueous acetonitrile (ACN) containing 0.1% TFA and acidified with formic acid (1% final). Peptides were extracted using StageTips (Rappsilber et al., 2007) and then analyzed in single nanoLC-MS/MS runs.

LC-MS/MS and data analysis*:* Peptides were separated on a Thermo-Dionex RSLCNano UHPLC instrument (Sunnyvale, CA) with 10 cm long fused silica capillary columns made in-house with a laser puller (Sutter, Novato CA) and packed with 3 µm 120 Å reversed phase C18 beads (Dr. Maisch, Ammerbuch, DE). The LC gradient was 90 min long with 10-35% B at 200 nL/min. LC solvent A was 0.1% acetic acid and LC solvent B was 0.1% acetic acid, 99.9% ACN. MS data was collected with a Thermo Orbitrap Elite spectrometer. Data-dependent analysis was applied using Top15 selection with CID fragmentation. Raw files were analyzed by MaxQuant/Andromeda (Cox et al., 2011) version 1.5.2.8 using protein, peptide and site FDRs of 0.01 and a score minimum of 40 for modified peptides, 0 for unmodified peptides; delta score minimum of 17 for modified peptides, 0 for unmodified peptides. MS/MS spectra were searched against the UniProt human and mouse databases (updated July 22nd, 2015). MaxQuant search parameters: Variable modifications included Oxidation (M). Carbamidomethyl (C) was a fixed modification. Max. labeled amino acids was 3, max. missed cleavages was 2, enzyme was Trypsin/P, max charge was 7, multiplicity was either 1, 2 or 3, SILAC labels were Arg0/Lys0 (light), Arg6/Lys4 (medium), Arg10/Lys8 (heavy). The MaxQuant Re-Quantification feature was

enabled. The initial search tolerance for FTMS scans was 20 ppm and 0.5 Da for ITMS MS/MS scans. Data was further processed using the Perseus software package (version 1.5.2.6), the R environment, Origin Pro 8.0 and Microsoft Excel.

F. Pull-down assays to measure SH3 domain engagement

In vitro SH3 pull-down: **Formation of the kinase–inhibitor complex**. The kinase of interest (100 nM) and mammalian lysate (0.2 mg/ml) were diluted in immobilization buffer (50 mM Tris, 100 mM NaCl and 1 mM DTT, pH 7.5). A saturating amount of the inhibitor of interest (5 μM or 10 μM) was added to this kinase dilution. The mixture was allowed to incubate for 30 min before loading on the resin.

SH3 Pull-down*.* Forty microliters of a 50% slurry of SNAP-Capture Pull-Down Resin (NEB) was placed in a microcentrifuge tube. The resin was washed (twice, ten-bed volumes) with immobilization buffer. A SNAP tag–polyproline peptide fusion (VSLARRPLPPLP) (10 μM) was loaded onto the resin at a final volume of 100 μl in buffer. The resin was rotated at room temperature for 90 min. After polyproline peptide immobilization, the resin was washed (twice, ten-bed volumes), and 100 μl of the kinase–inhibitor complex was loaded. The resin was allowed to shake at room temperature for 1 hr. After incubation with the kinase–inhibitor complex, the flow through was collected, and the resin was washed (three times, ten-bed volumes). To elute the retained kinase, 100 μl of 1× SDS loading buffer was added, and the beads were boiled at 90 °C for 10 min. All samples were separated by SDS-PAGE and visualized by western blotting using a His6-specific

antibody (at a 1:5,000 dilution (abm, HIS.H8)). The scanned blots were quantified with LI-COR Odyssey software to determine the percentage of kinase retained on the resin on the basis of the loaded and eluted fractions (mean ± SEM, *n* = 3).

Cellular SH3 pull-down: Flp-In T-REx 293T cells engineered to overexpress Src^{AS}, Hck^{AS}, or Hck^{WT} upon induction with doxycycline (dox) were plated on 6-well plates and grown to 90% confluency before induction of protein expression with 0.5 μg/mL dox. After 18 hr dox-induction cells were treated with 10 μM **1**, **2**, or **3** (0.5% DMSO final) for 2 hrs before removal of media, 1x PBS wash, and lysis in 100 μL Mod. RIPA buffer (50 mM tris, 150 mM NaCl, 1% Igepal-630, 1 mM EDTA, 1x Pierce Protease Inhibitor Tablet (Pierce, product number 88266), and 1x Pierce Phosphatase Inhibitor tablet (Pierce, product number 88665), pH = 7.8) containing 10 μM of **1**, **2**, or **3** for 20 min on ice before clarification by centrifugation 17,000xg at 4°C. Cleared lysates were then added to SH3 domain-binding resin (prepared as described above), and incubated at room temperature for 1 hr, before beads were extracted and washed twice with Mod. RIPA buffer (containing 10 μM **1**, **2**, or **3**). After wash, retained kinase was eluted by addition of 50 μL 1x SDS loading dye and boiled for 10 min. Eluents were then separated by SDS-PAGE and visualized by wester blotting with anti-FLAG antibody (1:2000 dilution; M2, Sigma). Percent retained kinase was calculated by dividing retained signal, by input signal quantified using LiCor Odyssey software.

G. pTyr527 by Csk

Titrations of Hck and Src constructs starting at 1600 nM (2-fold serial dilutions, 4 data points) were incubated with 10 μM **2** or **3** in assay buffer (75 mM HEPES pH 7.5, 150 mM NaCl, 0.25 mg/mL BSA, 1mM Na_3VO_4, 1 mM DTT, 15 mM $MgCl_2$, and 3.75 mM EGTA). Following 1 hr incubation at room temperature, 50 nM Csk was added and phosphorylation was initiated by the addition of γ32P ATP (0.2 μCi/well). The final volume of each assay well was 30 μL. The enzymatic reaction was run at room temperature for 1 hr and then terminated by spotting 4.6 μL of the reaction mixture onto a nitrocellulose membrane. Membranes were washed with 0.5% phosphoric acid (3x, 10 minutes each wash), air-dried, and the radioactivity was determined by phosphorimaging with a GE Typhoon FLA 9000 phosphor scanner. The scanned membranes were quantified with ImageQuant and data was analyzed using Prism Graphpad software (mean ± SEM, *n* = 3).

H. Confocal microscopy to track SFK localization

24 hrs before transfection $4x10^4$ SYF cells, were plated onto 18mm glass cover slips (Fisher, 12-546) in a standard 12-well plate. After transfection with the appropriate Src construct (see section B for details) cells were allowed to recover for 24 hrs before treatment with 10 μM **3**, 3 μM **2**, or DMSO (0.5% DMSO final for all conditions). Cells were incubated with drug for 15 min before media was removed and cells were washed once with PBS. After the PBS wash was removed, cells were fixed in 4% paraformaldehyde prepared to 1x PBS (16% paraformaldehyde, Electron Microscopy Sciences 15710) for 10 min. Paraformaldahyde was then removed and the cells were washed twice with PBS before simultaneous staining with Nucblue (2 drops per mL; Fisher, NC0302873)

and Wheat Germ Agglutinin AlexaFluor-647 conjugate (1.5 μL/well of 1 mg/mL stock solution; Thermo, W32466) prepared in PBS (250 μL total volume per well). After staining, slides were mounted onto glass cover slips using Fluoromount G (Southern Biotechnology, 0100-01) and sealed. Images were generated using a Leica SP8X Confocal Microscope and appropriate wavelengths to visualize GFP, DAPI, and AF647.

I. Cell motility assay

Experiments were performed using the Cytoselect 24-well Cell Invasion Assay (Basement Membrane, fluorometric format, product number CBA-111). The invasion chamber plate was allowed to warm to room temperature for ten minutes before rehydration of basement membrane layer by addition of 300 μL warm, serum-free media to inner compartment. After 1 hr, the rehydration medium was removed and replaced with 300 μL of cell suspension ($1x10^6$ SYF cells transfected 24 hours previously with Src^{AS} in serum-free media) while 500 μL DMEM +10% FBS was placed in the lower well of the invasion chamber. 3 μM **2**, 10 μM **3**, or DMSO (0.5% final DMSO for all conditions) was added to the cell suspension before the plate was incubated at 37°C in a 5% CO_2 atmosphere. After 48 hrs, media was removed from the insert, and insert was transferred to a clean well containing 225 μL cell detachment solution and incubated for 30 min at 37°C. Cells were then dislodged from the underside of the membrane and the insert was discarded. 75 mL 4x Lysis buffer/CyQuant GR solution was then added to each well containing cells in detachment solution and incubated for 20 min at room

temperature, after which 200 μL of the mixture was transferred to a 96-well plate and read for fluorescence using a plate reader at 480nm/520nM (EnVision Perkin Elmer, 485nM/538nM filter).

References:

1. Lim, W. A. *Curr. Opin. Struct. Biol.* **2002**, *12*, 61–68.
2. Goreshnik, I. *J. Am. Chem. Soc*. **2009.** *132*, 938–940.
3. (a) Oltersdorf, T.; et al. *Nature* **2005**, *435*, 677–681. (b) Shoemaker, A. R.; et al. *Cancer Res.* **2006**, *66*, 8731–8739. (c) Wendt, M. D.; et al. *J. Med. Chem.* **2006**, *49*, 1165–1181. (d) Bruncko, M.; et al. *J. Med. Chem.* **2007**, *50*, 641–662.
4. Llambi, F.*; et. al. Molecular Cell,* 2011, *44*, 1–15.
5. Goreshnik, I.; et. al. *Bioorg. Med. Chem. Lett*. **2011.** *21*, 4951–4955.
6. *Chen, S.; et. al. Cancer Res.* **2007,** *67,* 782.
7. Goreshnik, I. *Unpublished Data*
8. Ghosha, K.; *Methods*. **2002**, *28,* 374–383.
9. Branda, C.S.; *Developmental Cell*, **2004,** *6*, 7–28.
10. (a) Cox,B.; *JARO*, **2012**. *13*, 295–322 (b) Hayashi, S.; *Developmental Biology* **2002**, *244*, 305–318
11. Liu, Y.; *PLoS ONE. **2010,*** 5.
12. Huh, WJ,; *Gastroenterology*. **2012**, *142*, 21-24.
13. Gibb, B. *Nucleic Acids Research*, **2010**, *38*(17), 5817–5832
14. Shoemaker, A.*; Cancer Res* **2006**, *66*, 8731-8739.
15. Bjelic, S.; *ACS Chem. Biol.*, **2013**, *8* (4), 749–757
16. Goreshnik, I.; et. al. *Bioorg. Med. Chem. Lett*. **2011.** *21*, 4951–4955.
17. Zhang, H.; et. al. *Ana. Biochem.* **2002,** 307 (1), 70-75.

18. Nicolas Jullien, FrancËois Sampieri**,** Alain Enjalbert and Jean-Paul Herman (2003) Nucleic Acids Research, Vol. 31, No. 2.

19. Jullien N, Goddard I, Selmi-Ruby S, Fina JL, Cremer H, et al. (2007) Conditional Transgenesis Using Dimerizable Cre (DiCre). PLOS ONE 2(12): e1355.

20. Amir Taslimi, Brian Zoltowski, Jose G Miranda, Gopal P Pathak, Robert M Hughes & Chandra L Tucker (2016) Nature Chemical Biology 12, 425–430.

21. Fuun Kawano Firisako Okazaki, Masayuki Yazawa & Moritoshisato (2016) Nature Chemical Biology 12,1059-1066.

22. Suzanne E. Schindler, Jordan G. McCall, Ping Yan, Krzystof L. Hyrc, Mingjie Li, Chandra L. Tucker, Jin-Moo Lee, Michael R. Bruchas & Marc I. Diamond (2015) *Scientific Reports* **5**, 13627

23. Kelly A. Zalocusky, Lief E. Fenno, and Karl Deisseroth, MD, PhD Current Challenges in Optogenetics